Quantitative Hydrodynamics Analysis of Left Ventricular Diastolic Dysfunction using Color M-Mode Echocardiography

Kelley Christine Stewart

Thesis Submitted to the faculty of the Virginia Polytechnic Institute and State University in partial fulfillment of the requirements for the degree of
Master of Science
In
Mechanical Engineering

Approved By:
Dr. Pavlos Vlachos, Committee Chair
Dr. Mark Paul
Dr. Mike Roan

October 8th, 2008
Blacksburg, Virginia

Keywords: Color M-Mode Echocardiography, Propagation Velocity, Spatial Pressure Distribution, Useful Filling Efficiency

A Color M-Mode Echocardiogram Investigation of the Hydrodynamics of Left Ventricular Diastolic Dysfunction

Kelley C. Stewart

Abstract

Numerous studies have shown that cardiac diastolic dysfunction and diastolic filling play a critical role in dictating overall cardiac health and demonstrated that the filling wave propagation speed is a significant index of the severity of diastolic dysfunction. However, the governing flow physics underlying the relationship between propagation speed and diastolic dysfunction are poorly understood. More importantly, currently there is no reliable metric to allow clinicians the ability to diagnose cardiac dysfunction. There is a greater need than ever for more accurate and robust diagnostic tools with the increasing number of deaths caused by this disease. Color M-mode (CMM) echocardiography is a technique that is commonly used in the diagnosis of Left Ventricular Diastolic Dysfunction (LVDD) and is used as the image modality in this work.

The motivation for the current work is a hypothesized change in the mechanism driving early diastolic filling. The early filling wave of a healthy patient is driven by a rapid early diastolic relaxation creating a pressure difference within the left ventricle despite the fact the left ventricular volume is increasing. As diastolic dysfunction progresses, the left ventricular relaxation declines and it is hypothesized that the left atrial pressure rises to create the favorable pressure difference needed to drive early diastole. This changes the mechanism driving early diastolic filling from a pulling mechanism primary driven by left ventricular relaxation to a pushing mechanism primarily driven by high left atrial pressure.

Within this study, CMM echocardiography images from 125 patients spanning healthy and the three stages of LVDD are analyzed using a newly developed automated algorithm. For the first time, a series of isovelocity contours is utilized to estimate the conventional propagation velocity. A critical point within the early filling wave is quantified as the point of early filling velocity deceleration. The clinically used propagation velocity is compared to a novel critical point propagation velocity calculated as a weighted average of the propagation velocities before and after the critical point showing an increase in the correlation between decreasing diastolic dysfunction stage and decreasing propagation velocity. For the first time the spatial pressure distributions calculated as the pressure relative to the mitral valve pressure at each location from the mitral valve to the ventricular apex, are quantified and analyzed at the instant of peak mitral to apical pressure difference for patients with varying stages of LVDD. The analysis of the spatial pressure distribution revealed three filling regions present in all patients. The pressure filling regions were used to calculate a useful filling efficiency with healthy patients having a useful filling efficiency of 64.8 ± 12.7% and severely diseased filling patients having an efficiency of 37.1 ± 12.1%. The newly introduced parameters and analysis of the CMM echocardiography data supports the hypothesis of a change in the mechanism driving early diastolic efficiency by displaying a decline in the early diastolic propagation velocity earlier into the left ventricle for severely diseased patients than for healthy filling patients and a premature breakup of the progressive pressure gradient fueling early diastolic filling in severely diseased patients.

Acknowledgements

First I would like to thank the National Science Foundation Graduate Research Fellowship for granting me funding for my current and future research endeavors. Thank you to my committee members Dr. Paul, Dr. Roan, and Dr. Grant and especially my committee chair and advisor Dr. Vlachos for your support and suggestions throughout this work.

Thank you to Dr. Little and Dr. Kumar at Wake Forest Baptist Medical Center for being my mentors throughout this process. You have given us the valuable insight into the medical field that helped to strengthen this work.

Thank you to my friends and colleagues in the AEThER Lab. A special thanks to John Charonko and Chris Weiland for your help and mentorship on this project.

Last but not least, I would like to thank my parents for consistently being a source of love, inspiration, and encouragement to me. Without their leadership I would not be the person that I am today.

Contents

List of Figures

List of Tables

Introduction

The motivation for the current work is a hypothesized change in the mechanism driving early diastolic filling. The early filling wave of a healthy patient is driven by a rapid early diastolic relaxation. In this period of relaxation, a pressure difference within the left ventricle is created despite the fact the left ventricular volume is increasing. This mitral to apical pressure difference created by the relaxation of the left ventricular during early diastole creates a suction effect within the left ventricle. A severely diseased left ventricle has decreased left ventricular relaxation leading to a reduced pressure difference between the left ventricular apex and left atrium which is inadequate to drive the early diastolic filling. For this reason it is hypothesized that the left atrial pressure must rise in severely diseased patients to create the pressure difference necessary for early diastolic filling. The increased left atrial pressure forces the blood from the high pressure left atrium to the lower pressure left ventricle. The increase in left atrial pressure creates a "pushing" effect driving early diastolic filling as opposed to the "pulling" effect in healthy early diastolic filling.

This thesis is contains two papers composed of work focused on the driving hypothesis introduced above. The two chapters have a limited amount of necessary overlap to allow the individual papers to be capable of being independently read and understood. The first chapter "A Methodology for Objective Quantitative Analysis of Color M-Mode Echocardiography," introduces a newly developed automated algorithm for the analysis of Color M-mode (CMM) echocardiogram images. Along with the introduction of the algorithm this paper focuses on the velocity analysis of CMM echocardiograms. The early filling waves used to calculate the propagation velocities are analyzed to quantify a point of deceleration within the early filling wave named the critical point. This unique critical point is used to calculate a novel critical propagation velocity. The current clinically used method for calculating the propagation velocity is compared to the critical propagation velocity to show an improvement in statistical significance among the stages of diastolic dysfunction.

The second chapter titled "Spatial Pressure Distribution and Useful Filling Efficiency Analysis" utilizes the automated algorithm introduced in chapter 1 and focuses on the pressure analysis of the CMM echocardiography images. For the first time, spatial pressure distributions which are the pressure relative to mitral valve pressure at each point within the ventricle from the mitral valve to the ventricular apex at the instant of peak mitral to apical pressure difference are analyzed for the varying stages of diastolic dysfunction. The waveforms are analyzed for their overall magnitude and shape as the patients' diastolic function declines. From this analysis of the spatial pressure distributions, the waveform is broken into three filling regions representing the different regimes of filling. A novel useful filling efficiency parameter is calculated using these filling regimes quantifying healthy left ventricular filling as much more efficient that severely restrictive filling.

The appendix is composed of two sections. Appendix A is an error analysis for this work composed of the error associated with the velocity reconstruction from CMM images and the error associated with the calculation of the critical point using the change-point analysis as well as a sensitivity analysis of the propagation velocity and pressure calculations. Appendix B is additional echocardiogram work in progress on additional efficiency analysis and formation number analysis.

1. A Methodology for Objective Quantitative Analysis of Color M-mode Echocardiography

Abstract

An automated algorithm was developed for the analysis of Color M-Mode echocardiography images to statistically analyze filling velocities and relative pressures along the length of the left ventricle. The newly developed algorithm includes a change-point analysis to quantify the most statistically significant change in the left ventricular filling dynamics. This statistical point of change within the filling velocities, named the velocity critical point is quantified in the E wave propagation velocity where ventricular filling is decelerated due to an adverse pressure gradient. The velocity critical point occurs at a greater normalized distance into the left ventricle for healthy patients (30.2 ± 8.1% of total left ventricular distance) and closer to the mitral valve location in severely diseased patients (14.4 ± 5.2% of total left ventricular length), in agreement with the hypothesis that the point of adverse pressure gradient occurs earlier in the ventricle as ventricular effectiveness decreases. From this velocity critical point, a critical propagation velocity is derived as a weighted average of the propagation velocity before the velocity critical point and the propagation velocity after the velocity critical point. This critical propagation velocity displays a stronger correlation with decreasing diastolic function then currently used clinical propagation velocity methods. The critical propagation velocity is also used to calculate a unique filling parameter to characterize the mechanism driving early diastole as the severity of diastolic dysfunction increases.

Nomenclature

A	**Peak transmitral A wave velocity**
A wave	**Diastolic atrial filling wave**
CMM	**Color M-Mode**
DD	**Diastolic dysfunction**
E	**Peak transmitral E wave velocity**
E wave	**Diastolic early filling wave**
E/A	**Transmitral peak velocity wave ratio**
E/E'	**Ratio of early transmitral flow velocity to early diastolic mitral annulus velocity**
EF	**Ejection Fraction**
LA	**Left Atrium**
LV	**Left Ventricle**
LVEDV	**Left Ventricular End Diastolic Volume**
LVESV	**Left Ventricular End Systolic Volume**
MV	**Mitral Valve**
PPD	**Peak Pressure Difference from the mitral valve to the apex**
ROI	**Region of Interest**
Vp	**Propagation Velocity**

Introduction

Diastolic dysfunction and diastolic heart failure are conditions that affect the filling dynamics of the heart. The first portion of diastole, early diastole or the E wave, is controlled by the relaxation of the left ventricular wall, creating suction and pulling blood from the left atrium (LA) into the left ventricle (LV) through the mitral valve (MV). Late diastole, A wave, is the second portion of the filling process where the LA contracts and forces blood from the LA into the LV. Many cardiovascular conditions including coronary artery disease, hypertension, Fabry disease and restrictive cardiomyopathy show signs of impaired relaxation of the LV [1, 2]. This condition decreases the effectiveness of early diastole, forcing an increase in the atrial contraction to compensate for the reduced filling during early diastole.

The introduction of the color M-mode (CMM) echocardiography represents a significant contribution towards understanding left ventricular filling in both healthy and diseased conditions. The CMM echocardiograph is currently the most useful clinical tool for diagnosis and understanding of cardiac function [3]. Unlike the classic Doppler echocardiography which allows for velocity measurements at only a single position, the color-M-mode echocardiography allows users to view velocities along a scanline from the mitral valve to the apex and over a specified time frame [4]. This method enables the noninvasive calculation of the propagation velocities and intraventricular pressure differences from the mitral valve to the ventricular apex along each time step using the Euler Equation [5-8].

One parameter that is commonly calculated from CMM images is the propagation velocity which measures the speed of blood traveling toward the apex during diastole. The magnitude of this velocity has been shown to correlate with the function of the filling of the left ventricle and is also related to wall relaxation [4]. A high velocity generally indicates healthy E wave filling and a reduced velocity generally corresponds to diseased filling conditions. The effectiveness of diastolic relaxation is directly related to propagation velocity [9]. Unfortunately, current methods of calculating propagation velocity (Vp) are sometimes inconclusive and inconsistent as a diagnostic tool for diastolic dysfunction [10].

Brun et al. first determined the propagation velocity of early diastolic filling using color M-mode echocardiography images. This propagation velocity was established by tracking the slope of a line fit to the leading edge of the E wave, where the color M-mode image velocity contour begins [4]. Similarly, the propagation velocity is often found by measuring the slope of the first color aliasing boundary on the CMM image [11]. Takatsuji et al. determined the filling wave propagation velocity from color M-mode images using a more complex method. The slope was determined by the point of maximum velocity at the mitral valve and the point at the mid ventricle where the velocity decreased to seventy percent of the maximum velocity [12]. In studies by Yotti et al. and by De Mey et al. the propagation speed was found by creating a line along the fifty percent isovelocity contour on the leading edge of the E wave[6, 13]. The majority of these methods are manual and dependent upon the interpretation and experience of the clinician performing the test [3]. A semi-automated approach was proposed by Stuggard et al. using eigenvector analysis of the CMM E wave to calculate the principal components and reconstruct an ellipse representing the E wave. The angle of rotation of the ellipse was calculated to determine the propagation velocity [14]. The E wave and A wave propagation velocities have also been studied together to determine a diagnosis parameter based on the ratio of these velocities by Parthenakis et al. The study found a stronger correlation between the ratio of propagation velocities to stage of diastolic dysfunction than either of the propagation velocities individually [15].

In addition to the propagation velocity, other measured echocardiograph parameters have been utilized as diagnostic parameters. The ratio of peak transmitral E wave inflow velocity (E) to the peak transmitral A wave inflow velocity (A) was studied to show a biphasic pattern with E/A ratios lower than 1 corresponding to impaired relaxation in the early diastolic filling and E/A ratios higher than 2 representing restrictive filling patterns. This ratio of transmitral velocities is severely altered by age and heart rate and does not significantly distinguish healthy patients from pseudonormal patients [16-18].

The relationship between E wave peak transmitral flow velocity and the E wave mitral annulus velocity (E/E') from Doppler tissue imaging has also been used as an indication for diastolic dysfunction by estimating the LV filling pressures with fairly good success [19, 20]. Ommen et al. found that an E/E' value of less than 8 most likely corresponds to a patient with healthy LV diastolic pressures; whereas an E/E' value greater than 15 is associated with increased pressures [20, 21]. In Ommen's study the range of E/E' values between 8 and 15 showed great variability between healthy and elevated pressures. Diastolic suction, the intraventricular pressure difference between the ventricular apex and the atrium, is another important factor in LV function [5, 8, 13, 22]. This value is simply a difference in pressures and does not incorporate an overall rise in the ventricular and apical pressures.

Despite the great interest and previous efforts a reliable methodology for clinically understanding the decline of diastolic function is not available. Based on the previous research it is clear that there are several limitations in the current analysis of diastolic dysfunction using CMM echocardiography. There is no standardization of the clinical calculation of the propagation velocity and there is a debate about the proper estimation methods [10, 23, 24], which makes the comparison of Vp values from one study to another difficult. A statistical limitation also exists in the calculation of the propagation velocity. Most current methods for calculating Vp use a single isovelocity contour to estimate the linear slope. This method is subject to variations in the estimated propagation velocity based on the single isovelocity contour selected and a single isovelocity contour can be affected by noise or artifacts within the single contour. The result may be a calculated propagation velocity that is not representative of the overall E wave Vp. There are also very few studies that focus on the interplay between propagation velocities and pressure distributions using CMM echocardiography.

In this study an automated algorithm was developed to analyze CMM images and calculate the propagation velocities and pressure distributions of each patient. This algorithm reduces the introduction of subjective assessment of the user and allows for a more consistent analysis of CMM images. Within the newly developed algorithm, a series of isovelocity contours ranging from 45% to 55% are calculated. A 2^{nd} , 3^{rd} and 4^{th} order polynomial is fit to the series of isovelocity contours and the polynomial with the smallest coefficient of determination is selected to represent the ensemble contour. The linear slope is then fit to the ensemble contour to estimate the conventional propagation velocity. This method eliminates noise or artifacts associated with a single isovelocity contour to allow for the estimation of a propagation velocity representative of the entire inflow wave. The propagation velocities and pressure distributions calculated by the automated algorithm are analyzed simultaneously to more completely understand their relationship.

In addition, a novel parameter is introduced to quantify a critical point in both the propagation velocity and the spatial pressure distribution. Within this study a discontinuity in the velocity of the filling wave and the pressure gradients was observed. For the first time, this discontinuity was quantified using a statistical change-point analysis [25, 26]. From this CRItical Singularity Point (CRISP) methodology, a novel critical propagation velocity was derived using a weighted average of the propagation velocity before and after the critical point. This new parameter has a stronger correlation with decreasing diastolic dysfunction stage than methods currently used clinically to measure Vp.

A discontinuity in the early diastolic filling has been detected in previous works. A study by Sessoms et al. compared multiple previously introduced methods for calculating the propagation velocity and noted the curvilinear shape of the leading edge of the early diastolic filling wave of many diseased patients [27]. Quiñones discovered that patients with pseudonormal and restrictive filling often show a curved pattern caused by the deceleration of blood as it moves further into the LV. This curved pattern in the diseased cases was observed but not quantified [23]. Asada-Kamiguchi et al. studied left ventricular aneurysms in sheep; ventricular flow patterns were analyzed and intraventricular pressure differences were calculated. In sheep with LV aneurysms a sharp disruption in the propagation velocity was observed, which was uncharacteristic of healthy sheep. It was determined that this change

in propagation velocity was due to a sudden decrease in velocity at the location of the aneurysm. The location of the velocity change was therefore used to determine the position of the aneurysm within the ventricle [28].

In this study, a methodology for calculating the velocity and pressure critical point is introduced and the critical point for both the E wave propagation velocity and spatial pressure distribution is quantified and studied. From this analysis a novel critical propagation velocity is introduced and compared to currently used clinical parameters.

Methods

Patient Population

Patients for the study were randomly and anonymously selected after echocardiograph and Doppler images were acquired at Wake Forest University Baptist Medical Center during regular examinations. Routine analysis on the Color M-mode images was completed and the propagation velocity was calculated. Diastolic dysfunction stages were assigned by cardiologists according to the ACC/AHA guidelines [29]. The patient population was selected based on the cardiologist diagnosed stage of diastolic dysfunction as well as the patients having no other pre-existing cardiac conditions. The E wave and A wave peak transmitral velocities (E and A) as well as the E' parameters were clinically calculated using pulse wave and tissue Doppler imaging. Five patient categories were used in this study. The first two categories were healthy patients, one group younger than thirty years old and the second group thirty years and older. The remaining three categories were composed of all ages of each of the three diseased stages: delayed relaxation filling, pseudonormal filling, and restrictive filling. Twenty-five patients were included in each of the five categories displayed in Table 1.1.

Table 1.1: Clinical Characteristics

Diastolic Dysfunction Stage	Number of Patients	Age	E/A	E/E'	Ejection Fraction
0 – Healthy, age < 30 yrs	25	23.81±5.43	1.85±0.79	6.87±1.65	0.58±0.05
0 – Healthy, age > 30 yrs	25	43.56±14.39	1.59±0.34	8.08±2.52	0.61±0.05
1 – Delayed Relaxation	25	69.35±9.67	0.78±0.12	12.86±4.36	0.59±0.10
2 - Pseudonormal	25	66.33±13.52	1.57±0.31	16.14±5.46	0.39±0.15
3 – Restrictive Filling	25	60.92±19.16	2.76±1.28	18.58±7.14	0.28±0.07
* Values represent mean value ± 1 standard deviation.					

A total of one hundred twenty-five patients were involved in the study. This study was conducted according to protocols approved by the Virginia Tech and Wake Forest University Internal Review Boards.

Statistical Analysis

All calculated properties were averaged for each category and are expressed as mean ± 1 standard deviation. The categories were compared using the nonparametric Wilcoxon rank-sum test and statistical significance between groups was determined using the Tukey-Kramer honest significant difference test at a significance level of 0.05. JMP Statistical Discovery Software was used for all statistical analysis.

Variability graphs shown in the analysis display a variable plotted versus diastolic dysfunction stage. The plots display individual patient values as discrete points vertically arranged above their corresponding diastolic stage labels. The mean diamonds are shown for each stage, with the center representing the group mean and the top and bottom points represent the 95% confidence intervals. Similarly, the box and whisker plot is shown. The center line within the rectangle represents the group median value, the top and bottom lines creating the rectangle are the 75% and 25% percentiles respectively.

Description of the Automated Algorithm

An automated data analysis algorithm was developed to determine the propagation velocity and pressure distributions from physiologic CMM echocardiograph images. Original color M-mode images are analyzed in Matlab using in-house developed image processing algorithms. The steps of this algorithm are discussed and referenced to a representative stage 3 restrictive filling patient for clarification. From the original CMM image, Figure 1.1A, the image region corresponding to the velocity color scale is manually selected. The color scale is then analyzed for its red, green, and blue color values before a cubic spline is fit to the color scale values. A rectangular region of interest (ROI) including a complete diastolic cycle is manually selected from the CMM image, shown in Figure 1.1B. From this ROI a point within the E wave and a point on the A wave, and the vertical position of the mitral valve tips are manually selected for orientation of the algorithm for the remainder of the analysis. The grayscale values from the CMM image background is automatically removed, thus leaving only the velocity color scale image, Figure 1.1C. Color scale cubic spline values are then used to create a point by point velocity reconstruction of the remaining image. This is necessary because the raw velocity data is unavailable and must be recreated from archived images.

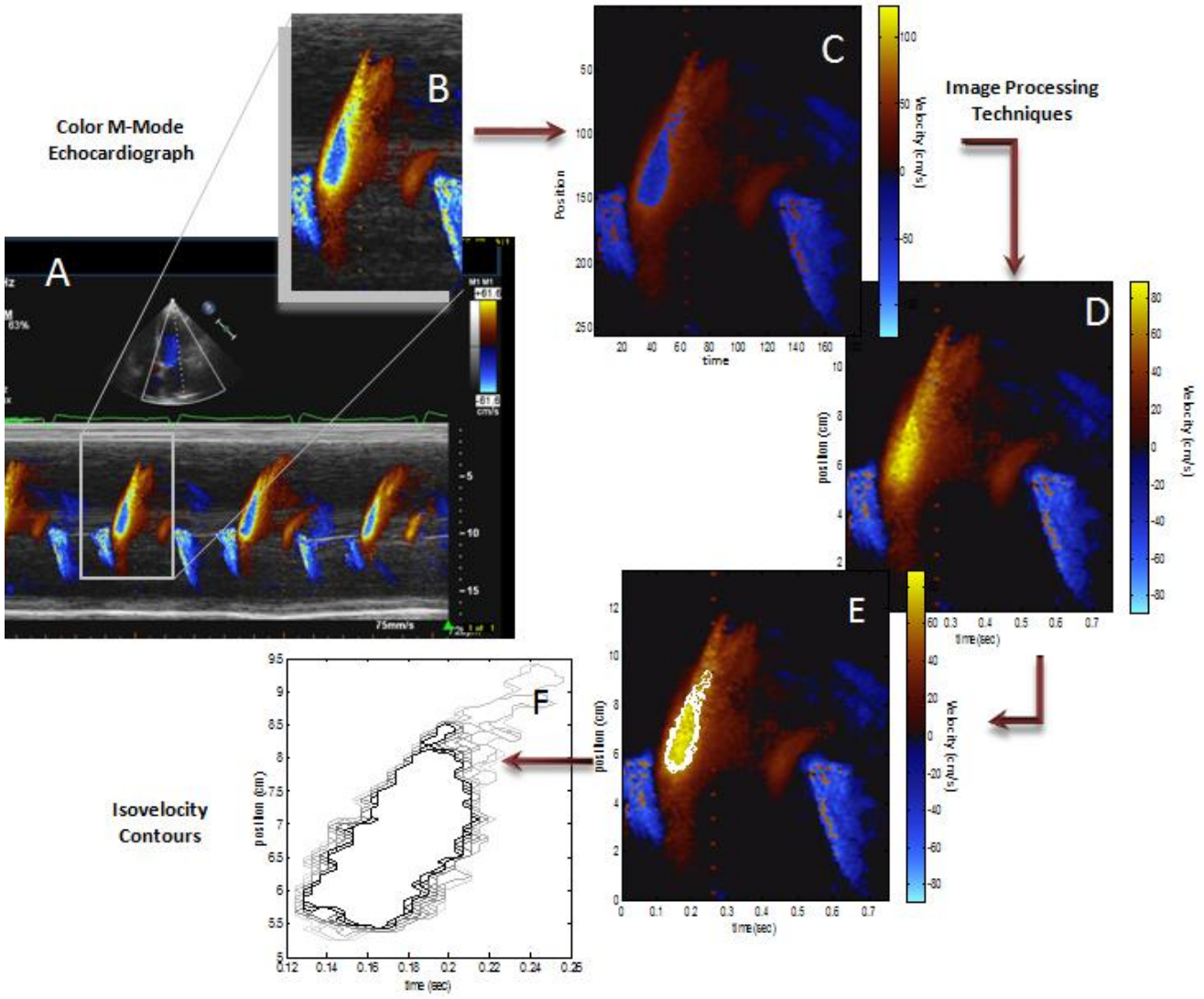

Figure 1.1: Color M-Mode Region of Interest of a Stage 3 restrictive filling patient displaying anti-aliasing techniques

A de-aliasing technique similar to the techniques used by Thomas et al. and Rovner et al. [30, 31] was used to reconstruct the image shown in Figure 1.1D. Through the use of image processing tools, the E wave velocity field is reduced to a series of twenty-seven isovelocity contours ranging from forty-five to fifty-five percent of the E wave transmitral velocity, shown in Figure 1.1E. The reconstructed velocity contours are shown in Figure 1.1F with the 45% to 55% isovelocity contours shown from light to dark.

Pressure Calculations

The reconstructed de-aliased velocity fields, also shown in Figure 1.1D, are also used to calculate the pressure fields by integrating the Navier-Stokes equation assuming one-dimensional incompressible flow:

$$\frac{\partial p}{\partial s} = -\rho\left(\frac{\partial v}{\partial t} + v\frac{\partial v}{\partial s}\right) + \mu\frac{\partial^2 v}{\partial s^2} \qquad 1.1$$

This equation calculates a pressure gradient as the sum of the acceleration and viscous terms, where P is the pressure, ρ is a constant density, u is the velocity vector, t is the time, and μ is a constant dynamic viscosity. The pressure difference between two points along the same CMM scanline can be calculated as a line integral between them. The entire pressure field relative to the ROI mitral valve tip location is calculated integrating to each point along a single scanline [32]. The velocity values measured by the CMM along the scanline are one dimensional velocities extracted from a three dimensional flow field, therefore the magnitude of these velocities may be incorrect because no out of plane velocities are captured. The inaccuracy of the velocity measurements will be propagated to the calculated relative pressures.

Once the pressure field is reconstructed, instantaneous pressure distributions along a scanline are analyzed. The change in pressure with respect to space, Δp/Δx is plotted in Figure 1.2A. The pressure difference from the mitral valve to the apex is calculated in plotted in Figure 1.2B. This is used to determine the instants of maximum ΔP for both the E and A waves. Once the time of the E wave peak pressure difference (PPD) from the mitral valve to the atrium is determined, the spatial pressure waveform can be resolved, Figure 1.2C. The spatial pressure waveform is the pressure at a single time instant, relative to the mitral valve tip pressure at each position along a line from the mitral valve tips to the apex. A series of seven spatial pressure waveforms are generated at the time-steps centered on the time of the PPD.

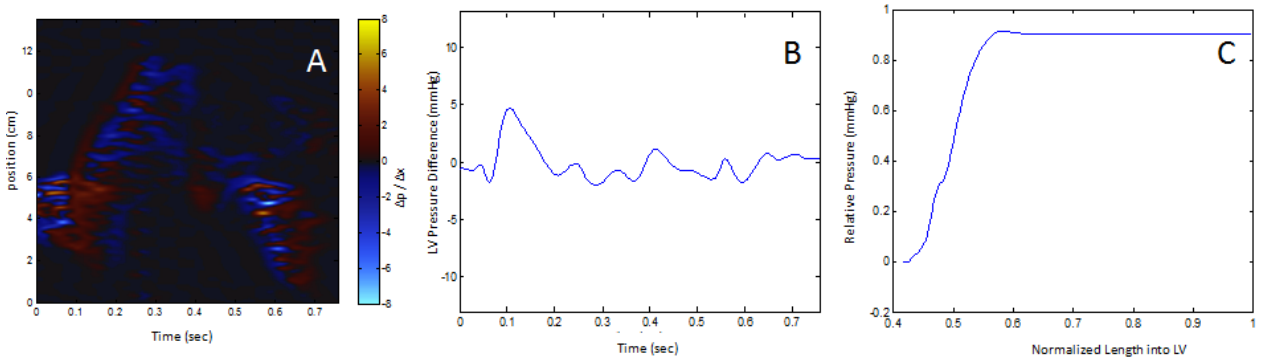

Figure 1.2: Pressure Distributions

Ensemble Contour Methodology

Many previous CMM echocardiography studies estimated the propagation velocities based on a single isovelocity contour of the E wave [3, 4, 11]. A single isovelocity contour has a possibility of noise or artifacts associated with it that may produce a propagation velocity estimate that is not characteristic of the entire filling wave. In this analysis, a series of contours is used to statistically reconstruct an ensemble contour to eliminate the noise or artifacts associated with individual waveforms. Error analysis of 25 representative patients spanning the five categories considered in this study revealed twenty-seven velocity waveforms and seven spatial pressure waveforms as the optimal numbers to use in the ensemble contour reconstructions. These numbers ensured that in all representative cases there was no more than a 1% change in r^2 values with an increasing number of waveforms. For both the propagation velocities and the spatial pressures a series of temporal or spatial waveforms respectively was created for each patient. A 2^{nd} , 3^{rd}, and 4^{th} order polynomial are sequentially fit to the series of waveforms. The best fit is selected based on the polynomial with the highest coefficient of

determination. The polynomial with the best fit is used in the remainder of the analysis as the ensemble contour.

The velocity ensemble contour is fit to the waveforms representing the leading edge of the isovelocity contours from the mitral valve tip location to the furthest point into the ventricle, shown in Figure 1.3A. A single linear slope fit to the velocity ensemble contour is representative of the conventional propagation velocity of the E wave. This conventional propagation velocity calculated by the algorithm is more statistically robust than previously introduced methods because the ensemble contour is calculated from a wide range of isovelocity contours to remove artifacts and noise. Figure 1.3B displays the seven spatial pressure contours and the ensemble spatial pressure contour plotted in bold. The spatial pressures are plotted as a relative pressure at a distance into the LV normalized by the total LV length.

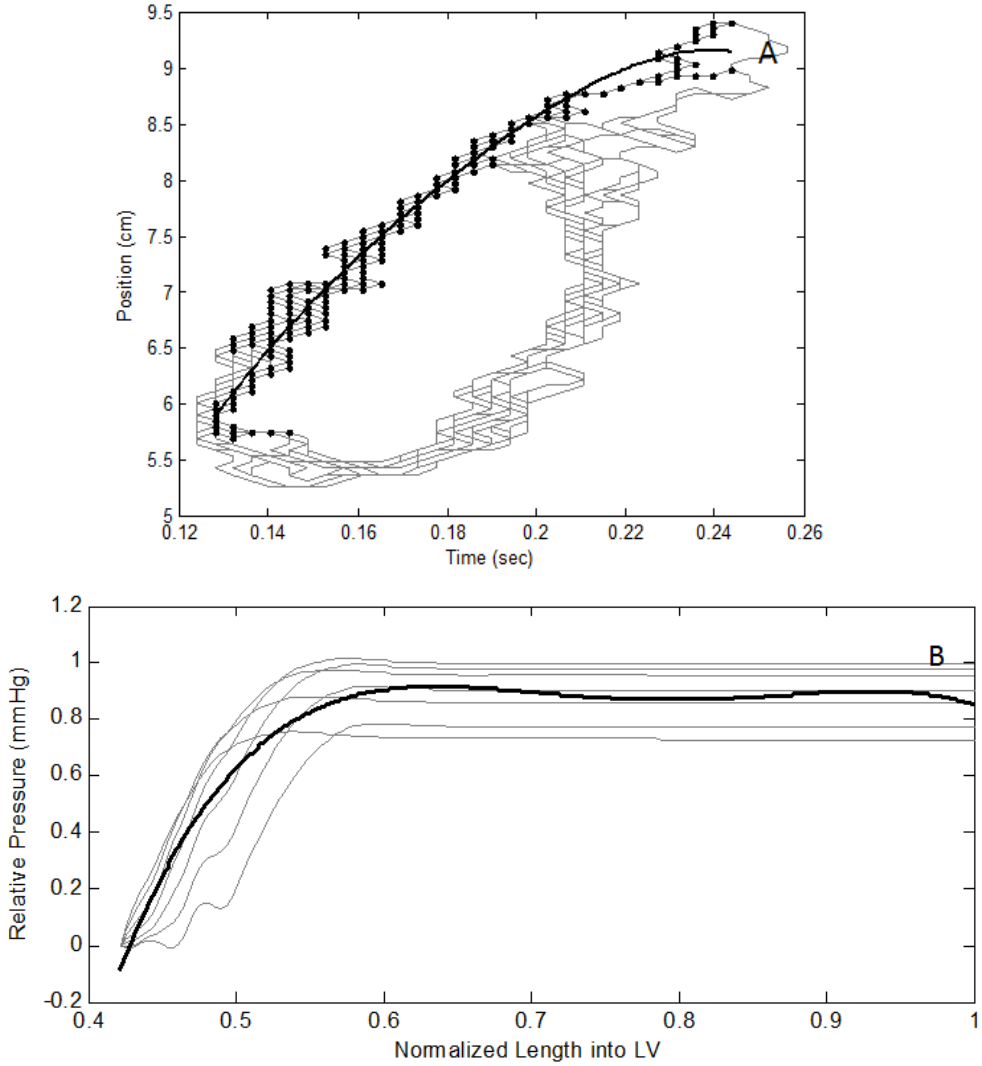

Figure 1.3: Ensemble Contours. A: Propagation velocity ensemble contour plotted on original isovelocity contours. B: Spatial pressure ensemble contour plotted on original spatial pressure contours.

Change-Point Methodology

Preliminary analysis of the isovelocity contours and spatial pressure waveforms revealed the consistent presence of a discontinuity within the velocity and pressure ensemble contours. Most often

after this initial break point, the slope was reduced or slowly decreased. This deceleration point was confirmed by previous researchers who also detected a change in slope or a curvilinear pattern to isovelocity contours [23, 27, 28]. In an effort to explore the physical significance of this variation, an algorithm was developed to deliver reliable and consistent estimation using a statistical change-point analysis that determines the most statistically significant change in the curve slope.

The change-point analysis is a statistical algorithm used to quantify the most statistically significant change along a waveform. The ensemble contours calculated in the Ensemble Contour Methodology section are used as the input waveforms for the change-point analysis. The change-point analysis was used on the ensemble contours to determine the point of the most statistically significant change within the waveform. The method is based on a cumulative sum of the difference between the value of interest, x_i, and the mean value, $\bar{x}$. Equation 1.2 displays the cumulative sum equation

$$CumulativeSum_i = CumulativeSum_{i-1} + (x_i - \bar{x}) \quad 1.2$$

The waveform produced by the output of the cumulative sum equation is then plotted to determine the significance of change throughout the signal [25, 26]. The peaks within this cumulative sum waveform are found and sorted according to their magnitude. The peak with the highest magnitude signifies the most statistically significant change. Any number of feasible change-points can be calculated and sorted based on significance using this method. In this work a single change-point, corresponding to the most statistically significant change is utilized. The most statistically significant change in the waveform is labeled as the critical point throughout this analysis. The ensemble contours for both the propagation velocity and spatial pressure ensure that a global change in the waveform is detected as the critical point. In 4 of the 125 patients, a statistical change in the velocity ensemble was not detected. These patients are excluded from all critical point analysis because the propagation velocity was too linear to detect a critical point.

Critical Propagation Velocity

The detection of a deceleration during the isovelocity contour used to estimate the propagation velocity signifies that a single straight line is not the optimal estimation for the propagation velocity. The critical point within the isovelocity contour represents a location where the slope of the isovelocity contour or the propagation velocity statistically decreases. For this reason, the isovelocity contour is divided at the critical point into the initial propagation velocity and the terminal propagation velocity. The portion of the filling wave before the velocity critical point is fit to a linear initial slope and the remaining portion of the ensemble contour is fit to a terminal linear slope. The novel critical propagation velocity can then be calculated as a weighted combination of the slope of propagation before and after the critical point using equation 1.3:

$$V_C = p_b S_1 + (1 - p_b) S_2 \quad 1.3$$

where p_b is the percentage of the waveform before the critical point and S_1 and S_2 are the propagation velocities before and after the velocity critical point, respectively.

Figure 1.4 displays a representative region of interest of a stage 3, restrictive filling, patient indicating the velocity critical point time and location, and the relative times and slopes for the initial propagation velocity and the terminal propagation velocity.

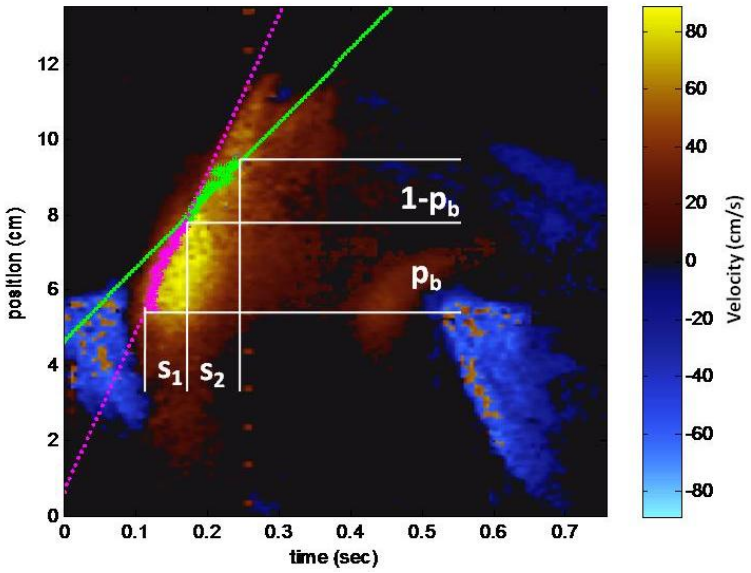

Figure 1.4: Critical Propagation Velocity Schematic

Results

The most commonly used parameter for the diagnosis of diastolic dysfunction using Doppler and CMM echocardiography is the E/E' ratio. Figure 1.5A displays the distribution of the E/E' parameter with respect to diastolic dysfunction stage for the patients included in this study using the clinically calculated E and E' values. In this variability plot the centerline of each diamond indicates the group mean value and the top and bottom apex of the triangle show the 95% confidence interval of the mean. The width of each triangle is related to the number of samples in each group. The centerline of the box and whisker rectangle indicates the median value for each group and the top and bottom lines of the rectangle display the 25th and 75th percentile values. The horizontal bars on the top of the image shows the groups with statistically different mean values. The healthy patients have very little E/E' scatter and the scatter substantially increases as the diastolic function declines. The distribution of this parameter for the patients within this study is in agreement with Ommen et al. and Paulus et al.'s works describing patients with an E/E' less than 8 as healthy and patients with E/E' greater than 15 as severely diseased. Unfortunately, the values between 8 and 15 need further parameters to distinguish their diastolic function [20, 33]. Paulus et al. refers to biomarkers or other echo Doppler derived parameters such as LV mass index or LA volume index to distinguish patients within this E/E' range as healthy or diseased [33]. It is important to note that this parameter is one of the major contributing factors to the clinical diagnosis of the diastolic dysfunction stage, and therefore this parameter may be inherently biased to have an increased correlation with diastolic dysfunction stage. Another commonly calculated parameter for the diagnosis of diastolic function is the E/A ratio, the ratio of the E and A wave transmitral velocities. The E/A ratio using clinically calculated transmitral velocities, Figure 1.5B, demonstrates a biphasic contour with delayed relaxation showing values below 1. These results are very similar to the published results by Bella et al. and Classens et al. which described diseased patients as E/A<0.6 or E/A>1.5. This parameter does not fully distinguish healthy from psuedonormal with both categories having an E/A ratio between 1 and 2 [15, 17] These two clinically used parameters are not independently adequate for understanding the physical decline of the LV filling. A more thorough investigation of the filling velocities and pressures associated with diastole is completed to analyze the changing physical parameters as the function of the LV during diastole diminishes.

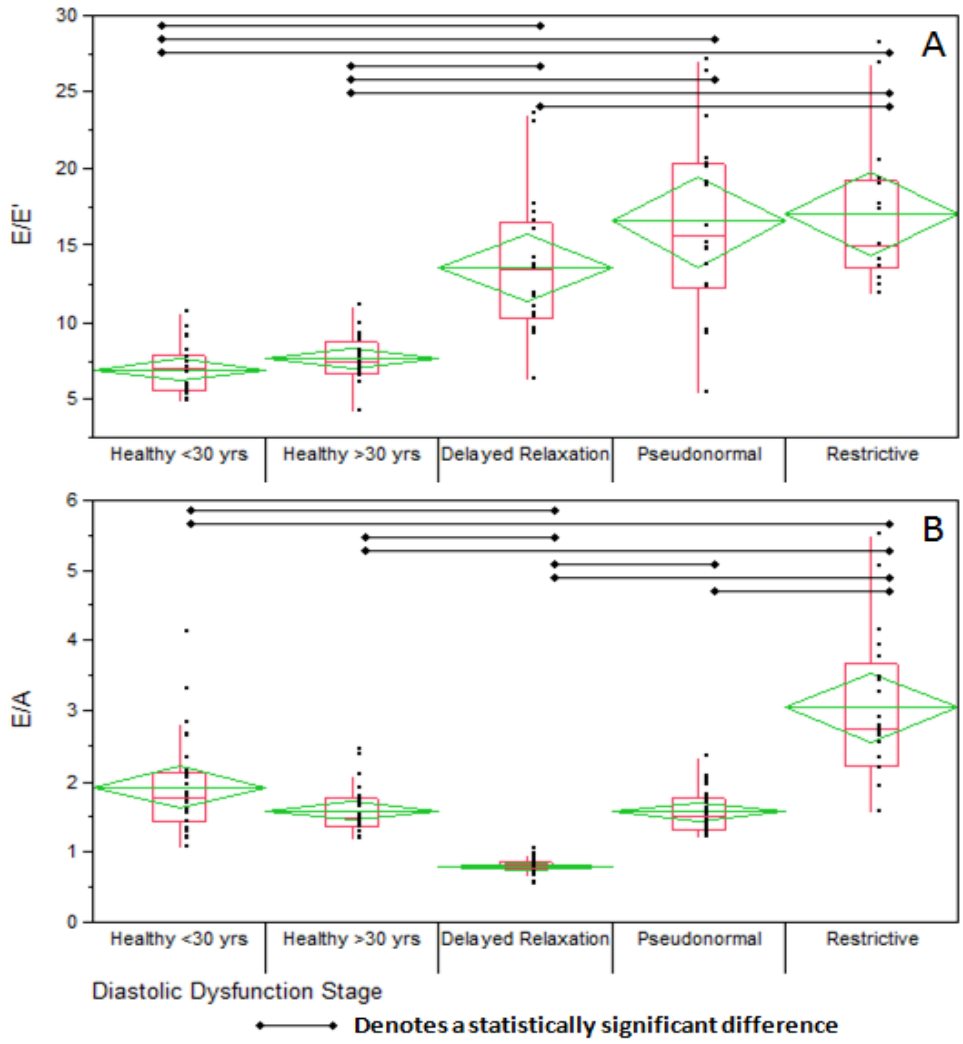

Figure 1.5: Clinically used Diagnostic Parameters plotted by Diastolic Dysfunction Stage

The E wave propagation velocity (Vp) can be calculated by cardiologists simply by viewing the CMM image using a technique described by Quiñones [23] using the first aliasing boundary to visually choose a single linear slope. This clinically used methodology is subject to the evaluator's interpretation, has high scatter, and low correlation with decreasing diastolic function, shown in Figure 1.6A. The conventional Vp calculated using the velocity ensemble contours discussed in the ensemble contour methodology section improves on the clinical methods. The ensemble contour is a statistical reconstruction of the isovelocity contours from 45-55%, eliminating the dependence on a single isovelocity contour and the aliasing boundary. The algorithm's improved methodology increases correlation with diastolic dysfunction stage and statistical significance of classifications but does not decrease the dispersion of values within each stage, shown in Figure 1.6B. Many researchers have discussed the physical changes as LV diastolic dysfunction worsens and presented substantial arguments implying the decline in propagation velocity due to the changes [3, 4, 9, 10, 34]. Unfortunately in the current analysis, both conventional methods of calculating the Vp do not demonstrate a substantial decline in Vp suggesting the current methods may not be completely capturing the velocity deceleration.

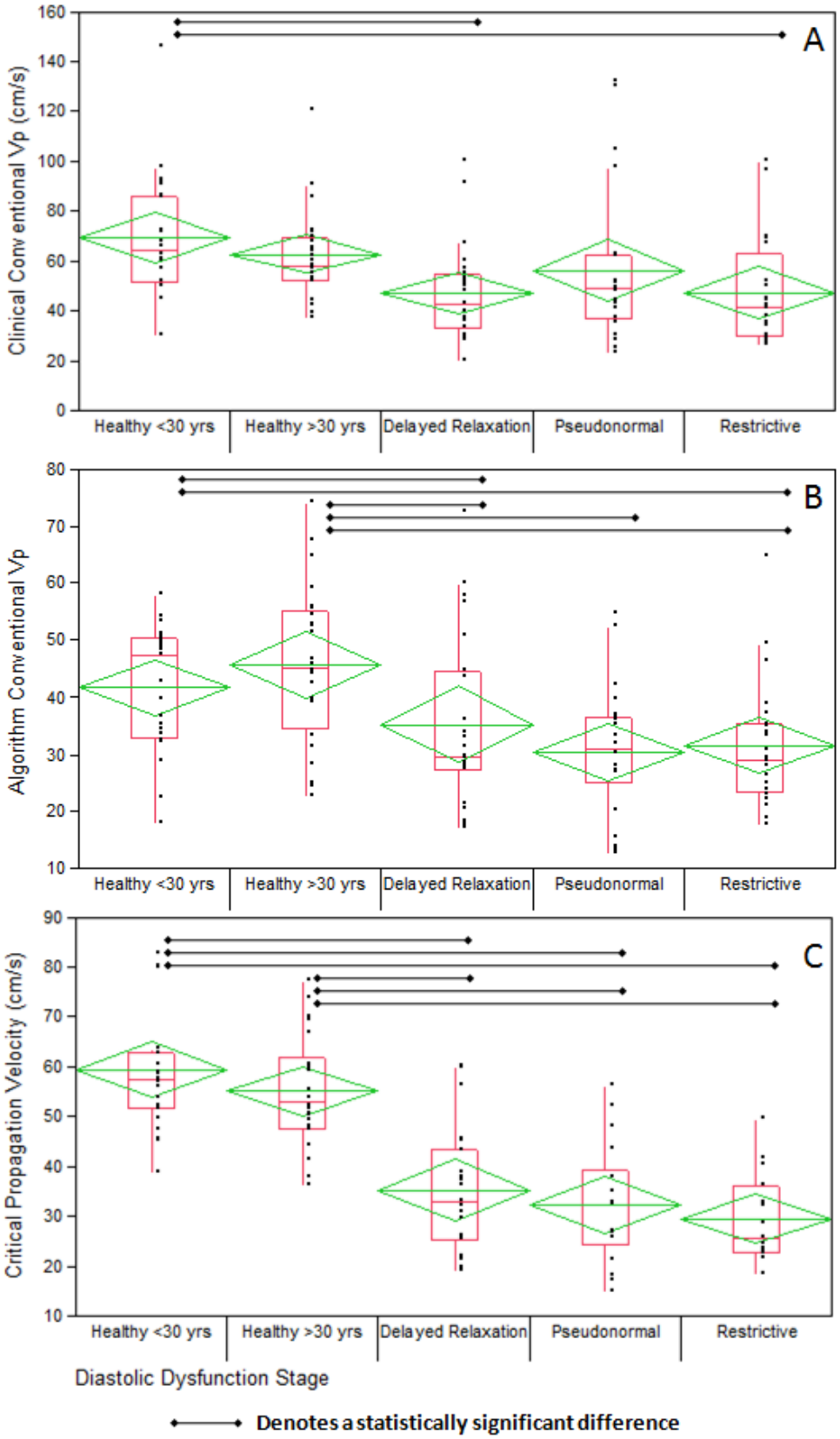

Figure 1.6: Comparison of Propagation Velocities

A discontinuity in the velocity ensemble contours was discovered during the ensemble contour analysis and a similar nonlinearity was observed by previous researchers [23, 27, 28]. It is hypothesized that the discontinuity in the velocity filling wave is caused by an adverse pressure gradient within the LV decelerating the flow.

The discontinuity and the associated velocity deceleration occur in both healthy and diseased patients. The critical point occurs the farthest into the LV for healthy patients and retreats towards the mitral valve as the diastolic function deteriorates. The velocity critical point location is related to the atrial pressure, LV relaxation, and LV compliance. The normalized location within the ventricle at which the velocity critical point occurs was calculated and is shown in Figure 1.7. The y-axis is the distance into the ventricle normalized by the total ventricular length. The healthy patients show a velocity critical point location later into the ventricle at 30.2 ± 8.1% into the LV while the restrictive patients have a velocity critical point location 14.4 ± 5.2% into the ventricle.

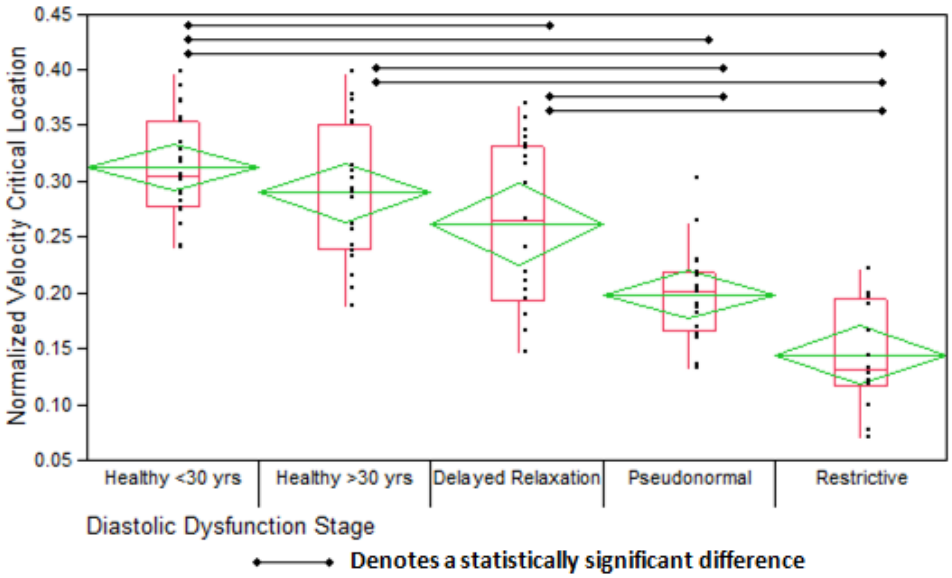

Figure 1.7: Normalized Distance into the LV where the velocity critical point occurs.

The deceleration of the propagation velocity in healthy patients occurs towards the end of the filling wave. Therefore, the clinical method for determining propagation velocity based on a single slope along the filling wave inlet is aimed towards healthy filling which more closely resembles a single linear slope. Figure 1.6C displays the critical point propagation velocity as a tool that facilitates a more complete tracking of the propagation of the fluid into the left ventricle during early diastolic filling. This parameter more closely tracks the decline of propagation velocity in diseased hearts to show a stronger correlation with diastolic dysfunction, an increased statistical significance between groups, and a decrease in individual group standard deviations as shown in Table 1.2.

The initial and terminal propagation velocities used to calculate the critical propagation velocity are compared in Figure 1.8. The initial propagation velocity, Figure 1.8A displays a weak correlation of initial Vp with diastolic dysfunction with large scatter in each stage. The terminal propagation velocity is fairly constant with mean values between 20 and 30 cm/s for all stages. The strong inverse correlation of calculated critical Vp with diastolic dysfunction is greatly dependent on the location of the critical point and therefore the weighted averages of these initial and terminal propagation velocities.

Table 1.2: Propagation Method Standard Deviations

	Clinical Conventional Vp	***Algorithm Conventional Vp***	***Critical Vp***
Healthy <30 yrs	*23.96*	*11.33*	*12.11*
Healthy > 30 yrs	*18.22*	*13.59*	*11.66*
Delayed Relaxation	*19.55*	*14.94*	*11.95*
Pseudonormal	*29.44*	*12.1718*	*11.37*
Restrictive	*22.97*	*9.41*	*9.66*

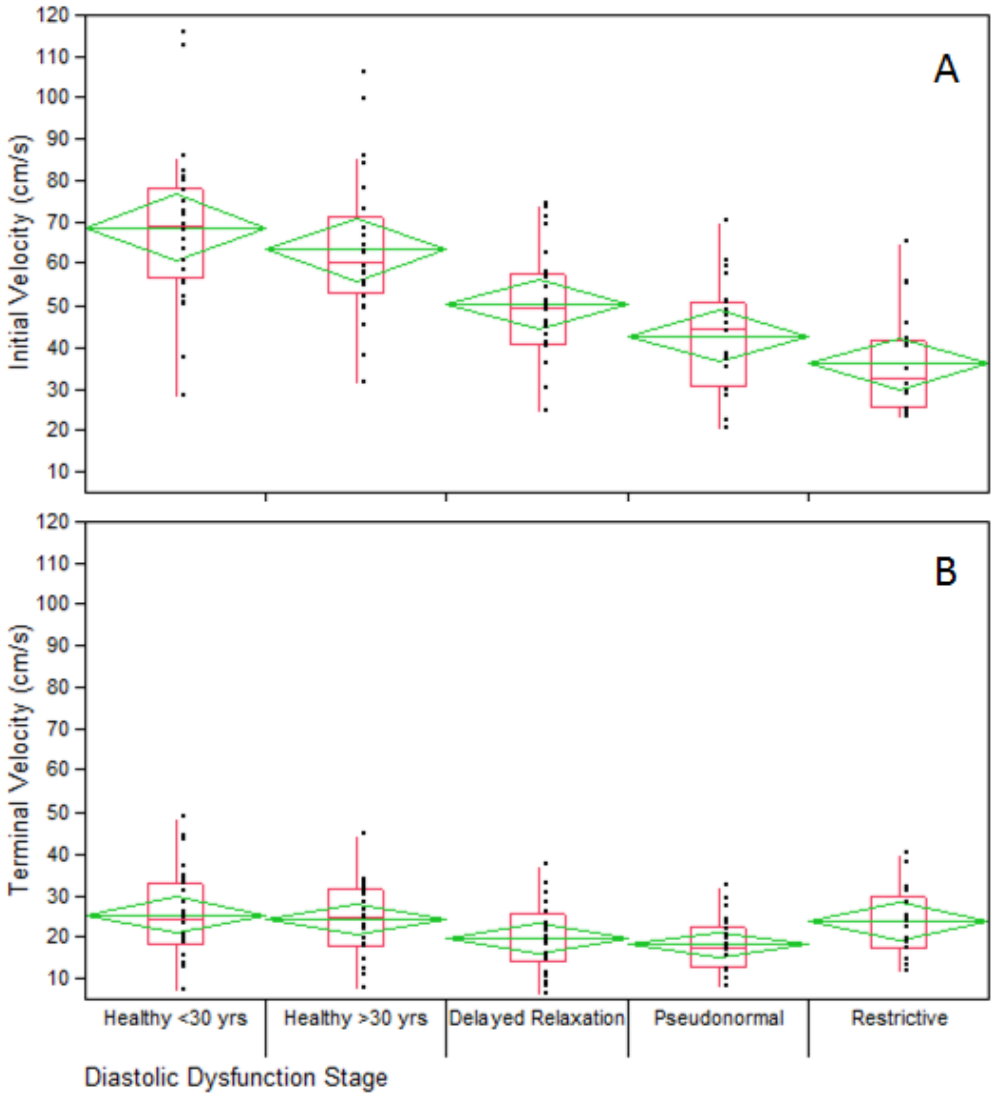

Figure 1.8: Comparison of Initial and Terminal propagation velocities

A significant index of the decline of diastolic function is a decrease in the mitral to apical pressure difference during diastole [13, 22, 35]. The filling pressure is a valuable parameter to study but the acquisition of absolute pressures within the left ventricle is a complex and invasive procedure [22]. This study used the Navier-Stokes equation to solve for the spatial pressure within the LV relative to the mitral valve at the time of E wave mitral to apical PPD. No absolute pressures are known but the relative pressures within the left ventricle display the magnitude of the difference between mitral and apical pressures.

The pressures within the LV relative to the mitral valve pressure, as discussed in the pressure calculation methodology section, are plotted in Figure 1.9. The waveforms shown are the calculated mean and median spatial pressure waveforms per category where the mean and median pressure magnitudes are calculated at each normalized location of the LV, which is the distance into the LV divided by total LV length. The x-axis represents the distance into the LV normalized by the total LV length. There is a trend of decreasing mitral to apical PPD as the stage of diastolic dysfunction increases and the shape of the waveform changes as the diastolic function decreases.

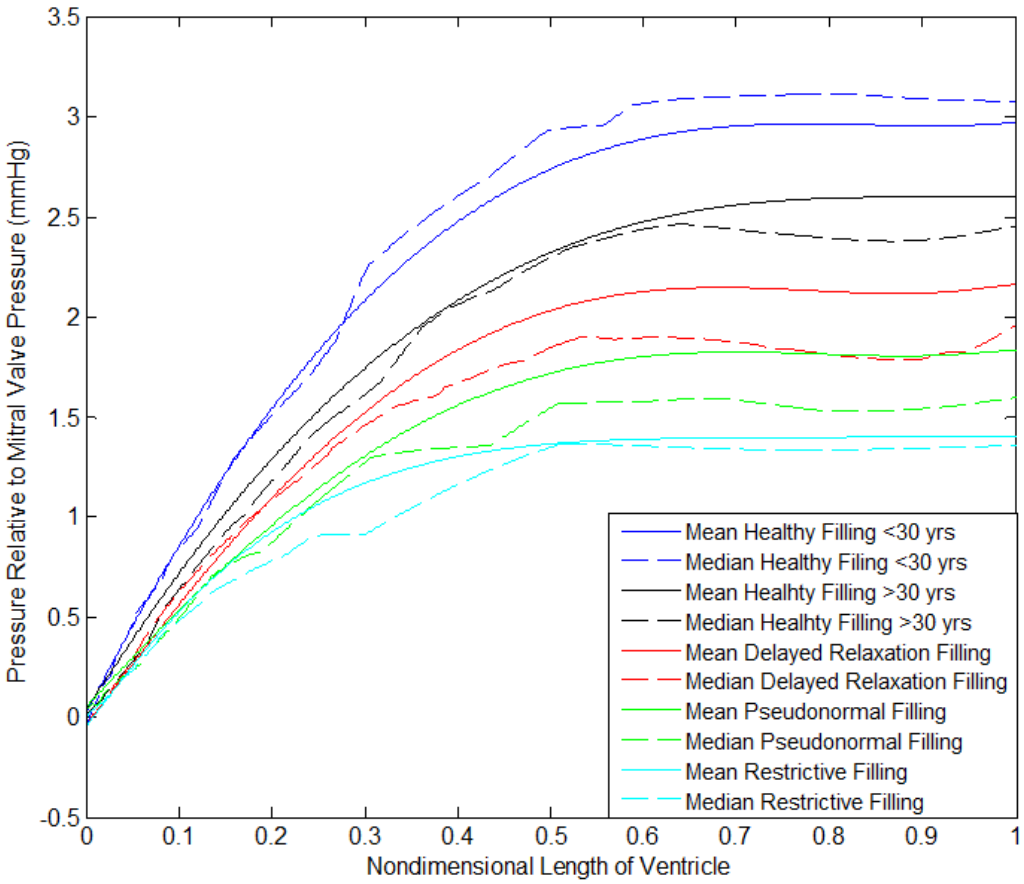

Figure 1.9: Spatial pressure distributions at the instant of peak mitral to apical pressure difference during early diastole

Discussion

The changes in the LV during the decline of diastolic function can drastically alter the physical characteristics of the LV. Overall ventricular compliance decreases, passive relaxation decreases, and filling pressures are changed. The heart is constantly adapting to its current state either causing or reacting to changes in these parameters. It is clear that the physical changes occurring in the heart may severely alter the efficiency of the LV's filling.

Healthy E wave filling is driven by LV relaxation causing suction within the LV and pulling blood from the LV towards the apex. A healthy heart is able to relax and create a large pressure difference between the mitral valve and the LV apex to complete early diastole without an increase in LA pressure [35]. The mean mitral to apical pressure difference for healthy patients within this study is 3.0 ± 1.0 mmHg, which is similar to the healthy pressure difference catheter measurements presented by Smiseth et al. [36] In these healthy patients, there is a point within the ventricle where the incoming blood flow is subject to an adverse pressure gradient and the blood velocity begins to slowly decelerate. In this study, the point of velocity deceleration for healthy patients occurs at 30.2 ± 8.1% of the total distance into the LV. The mean healthy initial velocity, before the critical point is 65.9 ± 18.5 cm/s and the velocity decreases at the critical point with a mean terminal velocity of 24.4 ± 10.2 cm/s. The calculated critical Vp, as discussed in the critical propagation velocity methodology section, for the healthy patients is 55.7 ± 11.5. The distance percentage of the initial velocity 61.5 ± 8.9 % of total filling distance is much greater than the distance percentage of the terminal velocity causing the calculated propagation velocity to more closely resemble the initial velocity.

A discontinuity in the E wave propagation velocity was observed in the velocity ensemble contours of severely diseased patients during the analysis of CMM images within this study. After investigating previous CMM propagation velocity studies, it was evident that earlier researches have observed this curvilinear shape or discontinuity in the Vp [23, 27, 28] even though the majority of propagation velocities are estimated with a single linear slope. As the heart becomes more diseased, the passive LV relaxation and the LV compliance reduce. The decline in LV passive relaxation is revealed in the decrease in mitral to apical peak pressure difference, 1.4 ±0.9 mmHg for the restrictive category, as the diastolic dysfunction stage increases, Figure 1.9. The ventricle's relaxation decreases causing a reduction in the suction driving early diastole, as a result the atrial pressure must increase to aid the blood into the stiffened ventricle. For this reason, the early diastolic filling changes from a suction driven filling to a positive pressure driven filling by pushing the blood into the LV. Blood entering the LV is met with an increased adverse pressure gradient shallower into the ventricle than healthy patients. The LV is not expanding at a healthy rate and the compliance is decreased so the fluid at the apex is relatively stationary. The location of the critical point is displayed in Figure 1.7, with the critical point of the restrictive cases occurring at just 14.1 ±5.3% into the LV. The initial velocity region of the early filling is shorter, representing 45 ± 10% of total filling distance with over half of the filling at the decelerated terminal velocity.

A new parameter calculated using the newly introduced critical point parameters is shown in Equation 1.4 and will be referred to as the Effective Stroke Length

$$Effective\ Stroke\ Length = \left(\frac{V_c}{d_{mv}f}\right)\left(\frac{L_{cp}}{L_{LV}}\right) \quad 1.4$$

Where Vc is the critical propagation velocity calculated in the critical propagation velocity methodology section, L_{CP} is the length into the ventricle where the velocity critical point occurs, d_{mv} is the diameter of the mitral valve, L_{LV} is the length of the left ventricle, and f is the frequency of the heartbeat in Hertz. This nondimensional parameter normalizes the propagation velocity and the effective length into the LV

at which the early wave velocity deceleration occurs with the patient specific filling parameters mitral valve diameter, left ventricular length and heart rate. The effective stroke length is plotted by diastolic dysfunction stage in Figure 1.10. As the diastolic function of the heart declines there is a decrease in propagation velocity and the distance into the ventricle at which the velocity critical point occurs. The decrease of these two parameters is linked to the adverse pressure gradients acting on the incoming flow not allowing the high velocity inflow to advance as far before deceleration. As these two normalized parameters decrease independently or simultaneously there is a decrease in the momentum contained in the early filling wave. There is a larger amount of scatter in the healthy patients and the scatter lessens as the diastolic dysfunction stage increases. As the LV declines the effective stroke length decreases to below 3 showing a low propagation velocity and severely decreased distance to velocity critical point.

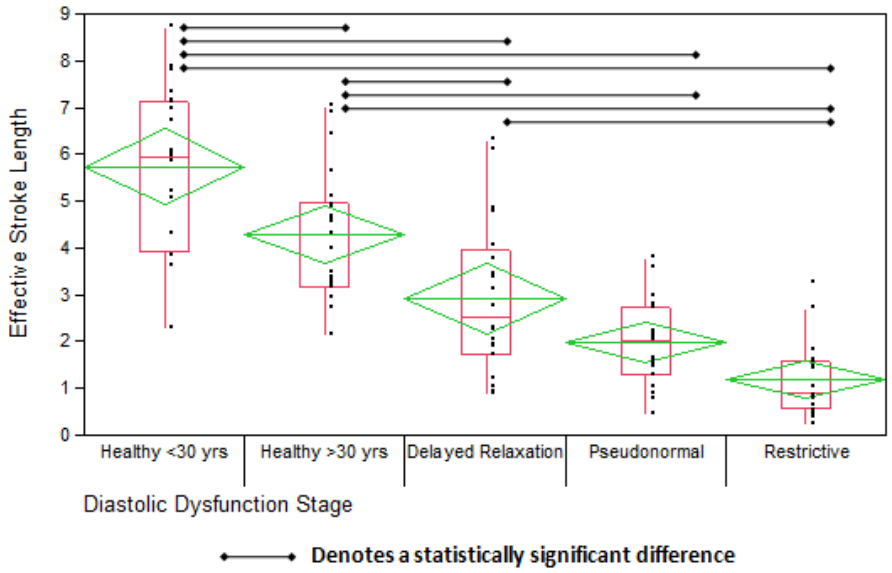

Figure 1.10: Effective Stroke Length derived from critical point parameters

Figure 1.11A displays this parameter plotted against the clinically used E/E' parameter. The colored contours define a one standard deviation prediction contour for each of the diastolic dysfunction stages, indicating a 68% chance of a patient falling within a contour is diagnosed as that stage. The E/E' parameter shows a dramatically increased scatter over the effective stroke length in the unhealthy cases and the reverse is true for the healthy cases. The border histograms show that there are very few patients with large effective stroke length and large E/E' values indicating a correlation between decreasing effective stroke length and increasing E/E' values. The rise of the E/E' parameter indicates a stiffening of the LV, where the E wave velocity remains fairly constant and the E' velocity decreases with declining diastolic function. The effective stroke length falls as diastolic dysfunction stage worsens due to a decline in the product of the propagation velocity and length of critical point indicating an increase in the strength of the adverse pressure gradient opposing flow. Figure 1.11B displays the same effective stroke length and E/E' values plotted as healthy or diseased patients. The contours indicate a one standard deviation prediction interval for healthy and diseased diagnosis. The healthy or diseased classification contours separate the two categories more accurately than either of the two tools independently.

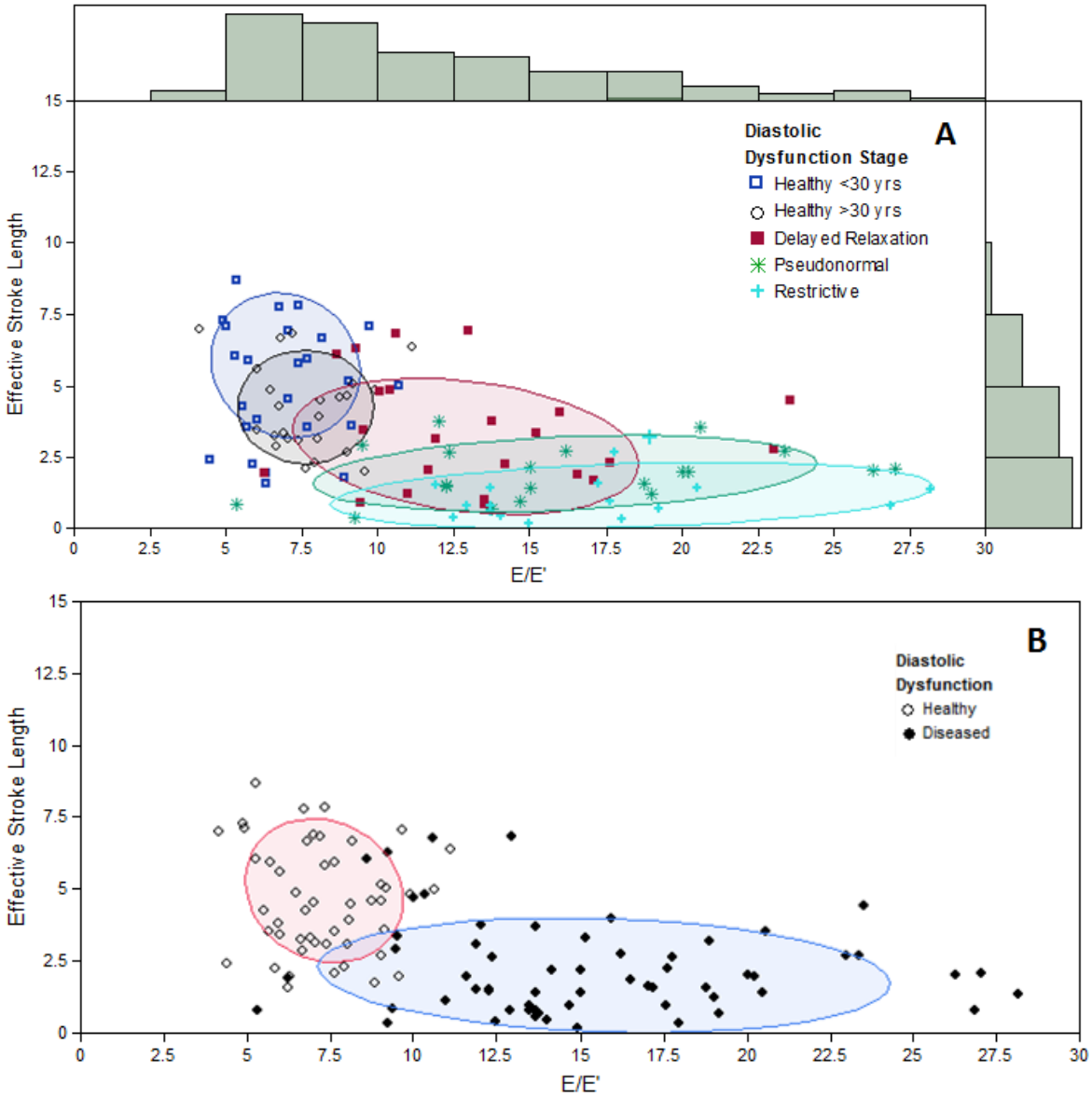

Figure 1.11: Effective Stroke Volume vs. E/E' Ratio

Conclusions

The velocity critical point and critical propagation velocity were introduced in this analysis as novel parameters for the analysis of CMM echocardiograph images. The critical point within the E wave is an important parameter in the analysis of early diastolic filling. This study was the first to quantify a critical location within early filling which is related to the early passive relaxation of the LV. Healthy filling patients have a velocity critical point occurring 30.2 ± 8.1 % of the total distance into the LV whereas restrictive filling patients' critical point occurs at only 14.4 ± 5.2% into the ventricle. The incoming blood travels at the initial velocity for half of the normalized distance in the severely diseased patients causing the calculated critical propagation velocity to be reduced.

The novel critical propagation velocity more closely tracks the decline of the incoming blood velocity and displays a much greater distinction between healthy and severely diseased patients than currently used clinical Vp methods. The novel critical Vp parameter is the first to use a weighted average of multiple propagation velocities. The parameters calculated from the critical point are included in the foundation of a unique effective stroke length, which has the potential to be used in collaboration with the E/E' parameter to characterize the decline of diastolic function. Future work involving BNP and clinical diastolic dysfunction survival studies should be completed to verify the correlations shown in this analysis.

References

1. Garcia, M.J., J.D. Thomas, and A.L. Klein, *New Doppler echocardiographic applications for the study of diastolic function.* Journal of the American College of Cardiology, 1998. **32**(4): p. 865-875.
2. Palecek, T., et al., *Early diastolic mitral annular velocity and color M-mode flow propagation velocity in the evaluation of left ventricular diastolic function in patients with Fabry disease.* Heart and Vessels, 2006. **21**(1): p. 13-19.
3. Oh, J.K., *Echocardiography in heart failure: Beyond diagnosis.* European Journal of Echocardiography, 2007. **8**(1): p. 4-14.
4. Brun, P., et al., *LEFT-VENTRICULAR FLOW PROPAGATION DURING EARLY FILLING IS RELATED TO WALL RELAXATION - A COLOR M-MODE DOPPLER ANALYSIS.* Journal of the American College of Cardiology, 1992. **20**(2): p. 420-432.
5. Greenberg, N.L., et al., *Estimation of diastolic intraventricular pressure gradients by Doppler M-mode echocardiography.* American Journal of Physiology-Heart and Circulatory Physiology, 2001. **280**(6): p. H2507-H2515.
6. De Mey, S., et al., *Assessment of LV Diastolic Filling Using Color M-Mode Doppler Echocardiography: Validation in a New Hydraulic Model*, in *Biomechan Model Mechanobiol*. 2004. p. 127-138.
7. Firstenberg, M.S., et al. *Semi-automated analysis of Color M-mode echocardiographic images for determining transmitral pressure gradients using a simplified Euler equation*. in *26th Annual Meeting on Computers in Cardiology*. 1999. Hannover, Germany.
8. Rovner, A., et al., *Relationship of diastolic intraventricular pressure gradients and aerobic capacity in patients with diastolic heart failure.* American Journal of Physiology-Heart and Circulatory Physiology, 2005. **289**(5): p. H2081-H2088.
9. De Boeck, B.W.L., et al., *Colour M-mode velocity propagation: a glance at intra-ventricular pressure gradients and early diastolic ventricular performance.* European Journal of Heart Failure, 2005. **7**(1): p. 19-28.
10. Thomas, J.D. and Z.B. Popovic, *Assessment of left ventricular function by cardiac ultrasound.* Journal of the American College of Cardiology, 2006. **48**(10): p. 2012-2025.
11. Moller, J.E., et al., *Ratio of left ventricular peak E-wave velocity to flow propagation velocity assessed by color M-mode Doppler echocardiography in first myocardial infarction - Prognostic and clinical implications.* Journal of the American College of Cardiology, 2000. **35**(2): p. 363-370.
12. Takatsuji, H., et al., *A new approach for evaluation of left ventricular diastolic function: Spatial and temporal analysis of left ventricular filling flow propagation by color M-mode Doppler echocardiography.* Journal of the American College of Cardiology, 1996. **27**(2): p. 365-371.
13. Yotti, R., et al., *A noninvasive method for assessing impaired diastolic suction in patients with dilated cardiomyopathy.* Circulation, 2005. **112**(19): p. 2921-2929.
14. Stugaard, M., et al. *Automated eigenvector analysis for quantification of color M-mode Doppler filling patterns of the left ventricle in an ischemic canine model*. in *24th Annual Computers in Cardiology Conference*. 1997. Lund, Sweden.
15. Parthenakis, F.I., et al., *Late left ventricular diastolic flow propagation velocity determined by color M-mode Doppler in the assessment of diastolic dysfunction.* Journal of the American Society of Echocardiography, 2004. **17**(2): p. 139-145.
16. Chapman, J.N., et al., *Intraventricular dispersion of E wave velocity: an alternative measure of left ventricular diastolic function in hypertensive patients?* Journal of Human Hypertension, 1999. **13**(12): p. 867-869.

17. Bella, J.N., et al., *Mitral ratio of peak early to late diastolic filling velocity as a predictor of mortality in middle-aged and elderly adults - The strong heart study.* Circulation, 2002. **105**(16): p. 1928-1933.
18. Galderisi, M., *Diastolic dysfunction and diastolic heart failure: diagnostic, prognostic and therapeutic aspect.* Cardiovascular Ultrasound. 2005. **3**(9).
19. Hillis, G.S., et al., *Noninvasive estimation of left ventricular filling pressure by E/e ' is a powerful predictor of survival after acute myocardial infarction.* Journal of the American College of Cardiology, 2004. **43**(3): p. 360-367.
20. Ommen, S.R., et al., *Clinical utility of Doppler echocardiography and tissue Doppler imaging in the estimation of left ventricular filling pressures - A comparative simultaneous Doppler-Catheterization study.* Circulation, 2000. **102**(15): p. 1788-1794.
21. Nagueh, S.F., et al., *Doppler estimation of left ventricular filling pressures in patients with hypertrophic cardiomyopathy.* Circulation, 1999. **99**(2): p. 254-261.
22. Thomas, J.D. and Z.B. Popovic, *Intraventricular pressure differences - A new window into cardiac function.* Circulation, 2005. **112**(12): p. 1684-1686.
23. Quinones, M.A., *Assessment of diastolic function.* Progress in Cardiovascular Diseases, 2005. **47**(5): p. 340-355.
24. Seo, Y., et al., *Assessment of propagation velocity by contrast echocardiography for standardization of color Doppler propagation velocity measurements.* Journal of the American Society of Echocardiography, 2004. **17**(12): p. 1266-1274.
25. Hinkley, D.V., *Inference about the Change-Point from Cumulative Sum Tests* Biometrika 1971. **58**(3): p. 509-523
26. Taylor, W.A., *Change-Point Analysis: A Powerful New Tool For Detecting Changes*. 2000.
27. Sessoms, M.W., J. Lisauskas, and S.J. Kovacs, *The left ventricular color M-mode Doppler flow propagation velocity V-p: In vivo comparison of alternative methods including physiologic implications.* Journal of the American Society of Echocardiography, 2002. **15**(4): p. 339-348.
28. Asada-Kamiguchi, J., et al., *Intraventricular pressure gradients in left ventricular aneurysms determined by color M-mode Doppler method: An animal study.* Journal of the American Society of Echocardiography, 2006. **19**(9): p. 1112-1118.
29. Hunt, S.A., et al., *ACC/AHA guidelines for the evaluation and management of chronic heart failure in the adult: Executive summary - A report of the American College of Cardiology/American Heart Association Task Force on Practice Guidelines (Committee to Revise the 1995 Guidelines for the Evaluation and Management of Heart Failure).* Journal of Heart and Lung Transplantation, 2002. **21**(2): p. 189-203.
30. Thomas, J.D., et al. *DIGITAL ANALYSIS OF TRANSMITRAL COLOR DOPPLER M-MODE DATA - A POTENTIAL NEW APPROACH TO THE NONINVASIVE ASSESSMENT OF DIASTOLIC FUNCTION*. in *Conf on Computers in Cardiology*. 1992. Durham, Nc.
31. Rovner, A., et al. *Improvement in diastolic intraventricular pressure gradients in patients with HOCM after ethanol septal reduction*. in *Annual Meeting of the American-College-of-Cardiology*. 2002. Atlanta, Georgia.
32. Charonko, J.J., P.P. Vlachos, and Asme. *Keynote paper: Time-accurate measurement of pressure from particle image velocimetry data*. in *5th Joint ASME/JSME Fluids Engineering Summer Conference*. 2007. San Diego, CA.
33. Paulus, W.J., et al., *How to diagnose diastolic heart failure: a consensus statement on the diagnosis of heart failure with normal left ventricular ejection fraction by the Heart Failure and Echocardiography Associations of the European Society of Cardiology.* European Heart Journal, 2007. **28**(20): p. 2539-2550.

34. Khouri, S.J., et al., *A practical approach to the echocardiographic evaluation of diastolic function.* Journal of the American Society of Echocardiography, 2004. **17**(3): p. 290-297.
35. Little, W.C., *Diastolic dysfunction beyond distensibility - Adverse effects of ventricular dilatation.* Circulation, 2005. **112**(19): p. 2888-2890.
36. Smiseth, O.A., et al., *Mechanics of intraventricular filling: study of LV early diastolic pressure gradients and flow velocities.* American Journal of Physiology-Heart and Circulatory Physiology, 1998. **44**(3): p. H1062-H1069.

2. Spatial Pressure and Useful Filling Efficiency Analysis

Abstract

The physiological changes within the left ventricle (LV) during the decline of diastolic function affect the filling pressure distribution throughout the LV. In this work, the spatial pressure distribution at the instant of E wave peak mitral to apical pressure difference is calculated based on Color M-mode echocardiography images. The analysis of the spatial pressure waveform across 125 patients spanning healthy and the three diseased stages of diastolic dysfunction reveals left ventricular filling regimes present in all spatial pressure distributions. The first is an initial filling region which is driven by the initial relaxation of the LV. This region is composed of a constant pressure gradient and the duration of this region is relatively constant ranging from 35.3 ± 4.5 % of the total left ventricular length for healthy filling patients to 26.2 ± 7.7% of the total LV filling length for severely diseased patients. The secondary region is a period of a decreasing pressure gradient as the LV relaxation slows. The secondary region is the location of the majority of differences between healthy and diseased filling. Healthy filling patients have a longer secondary filling region as the LV relaxation lessens and there is a smooth decline in the spatial pressure gradients. Oppositely, the severely diseased patients have a shorter secondary filling region and a more abrupt decline in pressure gradients due to abnormal or insufficiency LV relaxation. The final region is defined as a plateau region where the pressure gradient is relatively zero. Diseased patients reach the point of spatial pressure plateauing earlier than healthy filling patients ultimately leading to a less efficiency early filling wave. The useful filling efficiency for the patients was calculated by integrating the spatial pressure waveform and multiplying this by the total length of the LV. The healthy filling patients showed a useful filling efficiency of 64.8 ± 12.7% whereas the severely diseased patients had a useful filling efficiency of 37.1 ± 12.1%.

Nomenclature

A wave	**Diastolic atrial filling wave**
CMM	**Color M-Mode**
DCM	**Dilated Cardiomyopathy**
DD	**Diastolic dysfunction**
E wave	**Diastolic early filling wave**
LA	**Left Atrium**
LV	**Left Ventricle**
MV	**Mitral Valve**
PPD	**Peak Pressure Difference from the mitral valve to the apex**
ROI	**Region of Interest**
Vp	**Propagation Velocity**

Background

Color M-mode (CMM) Echocardiography has emerged as an extremely useful tool for the noninvasive assessment of patients with cardiovascular diseases including diastolic dysfunction. This technology allows users to measure the velocities within the left ventricle (LV) along a scanline often aligned with the mitral to apical inflow tract [1, 2]. The propagation velocities (Vp) and the early (E) and atrial (A) velocity magnitudes and durations can be calculated from CMM imaging. Brun et al. demonstrated a strong correlation between propagation velocity and wall relaxation, and he showed a trend of decreasing Vp and consequently wall relaxation as diastolic dysfunction increases [1, 3]. Diastolic function is dependent on the interplay among the LV relaxation, LV compliance, and filling pressures [4, 5]. The velocity scanlines at each time step within a diastolic cycle represent the spatiotemporal velocity distribution and can be utilized to calculate the pressure field by using the Euler equation [6-10]. This analysis results in relative pressures between the mitral valve location and the apical position of the LV.

Diastolic dysfunction is rated by severity from stage 0 being healthy filling to stage 3 being restrictive filling. As the diastolic function decreases the ventricular relaxation and left ventricular compliance decreases [9, 11]. In diseased patients, a decrease in the early diastolic relaxation in addition to a decreased compliance of the LV inhibits the LV from filling normally; the left atrium must increase its pressure and force the blood into the LV [6, 11]. For this reason, the pressures within the LV during the E wave are very important to understanding the fluid dynamics of early filling. Measuring pressure magnitudes within the LV is an invasive procedure and is not often performed in routine evaluations [12]. The intraventricular pressure difference between the ventricular apex and the atrium is more commonly calculated to evaluate LV function [13-17]. This value is simply a difference in pressures and does not incorporate an overall rise in the ventricular and apical pressures.

Many researchers have calculated left ventricular pressure differences (LVPD) described as the peak mitral to apical pressure difference. Yotti et al. calculated LVPD for healthy patients and patients with dilated cardiomyopathy. The healthy patients had a mean LVPD of 2.5 mmHg whereas the LVPD for patients with dilated cardiomyopathy was 1.2 mmHg [7]. Popović et al. calculated the LVPD in young healthy patients and sedentary elderly patients. The range of IVPG for young patients was 2-3 mmHg and the elderly sedentary patients had LVPD values just above 1 mmHg [16]. Smiseth et al. conducted an invasive catheter study to calculate the LVPD driving early diastole. The mean LVPD for eight healthy adult males was 3.5 ± 0.3 mmHg [18].

Yotti et al. presented the instantaneous pressure distribution at the time of peak LVPD to examine the spatial pressure distribution along the length of the LV for healthy patients and patients suffering from dilated cardiomyopathy (DCM). The LVPD for healthy patients was found to be larger than the LVPD for DCM patients. The filling pressure waveform was found to be different for the two filling types. The healthy have a constantly increasing pressure relative to the LV base along the ventricular length, whereas the DCM patients have a relative pressure that increased more suddenly and then remained constant for the remainder of the LV [7].

Many current studies of pressure distributions derived from noninvasive CMM measurements are limited by calculating the left ventricular pressure differences and not analyzing the spatial pressure distribution. Acquiring the absolute pressure measurement in the left ventricle is a very invasive procedure and is therefore not obtainable for common or preventative diagnosis. Although many researchers calculate the LVPD, this measurement does not necessarily capture the physical changes in filling from healthy to restrictive diastolic dysfunction filling.

The current study calculates the spatial pressure distribution for 125 patients spanning from healthy through all three stages of diastolic dysfunction. The instantaneous filling pressure waveforms at the time of the LVPD are analyzed and broken down into three stages of filling. This is the first analysis of the spatial pressure waveforms of diastolic dysfunction patients and the only study to

introduce and analyze the three filling pressure wave regions. The distribution of filling pressure stages is analyzed to introduce a novel efficiency parameter.

Methods

Patients for the study were anonymously selected after echocardiograph and Doppler images were acquired at Wake Forest University Baptist Medical Center during regular examinations. Routine analysis on the Color M-mode images was completed and the propagation velocity was calculated. Diastolic dysfunction stages were assigned by cardiologists according to the ACC/AHA guidelines [19]. The patient population was selected based on the cardiologist diagnosed stage of diastolic dysfunction as well as the patients having no other pre-existing cardiac conditions. The E wave and A wave peak transmitral velocities (E and A) as well as the E' parameters were clinically calculated using pulse wave and tissue Doppler imaging. Five patient categories were used in this study. The first two categories were healthy patients, one group younger than thirty years old and the second group thirty years and older. The remaining three categories were composed of all ages of each of the three diseased stages: delayed relaxation filling, pseudonormal filling, and restrictive filling. Twenty-five patients were included in each of the five categories displayed in Table 2.1.

Table 2.1: Clinical Characteristics

Diastolic Dysfunction Stage	Number of Patients	Age	E/A	E/E'	Ejection Fraction
0 – Healthy, age < 30 yrs	25	23.81±5.43	1.85±0.79	6.87±1.65	0.58±0.05
0 – Healthy, age > 30 yrs	25	43.56±14.39	1.59±0.34	8.08±2.52	0.61±0.05
1 – Delayed Relaxation	25	69.35±9.67	0.78±0.12	12.86±4.36	0.59±0.10
2 - Pseudonormal	25	66.33±13.52	1.57±0.31	16.14±5.46	0.39±0.15
3 – Restrictive Filling	25	60.92±19.16	2.76±1.28	18.58±7.14	0.28±0.07
* Values represent mean value ± 1 standard deviation.					

A total of one hundred twenty-five patients were involved in the study. This study was conducted according to protocols approved by the Virginia Tech and Wake Forest University Internal Review Boards.

Statistical Analysis

All calculated properties were averaged for each category and are expressed as mean ± 1 standard deviation. The categories were compared using the nonparametric Wilcoxon rank-sum test and statistical significance between groups was determined using the Tukey-Kramer honest significant

difference test at a significance level of 0.05. JMP Statistical Discovery Software was used for all statistical analysis.

Variability graphs shown in the analysis display a variable plotted versus diastolic dysfunction stage. The plots display individual patient values as discrete points vertically arranged above their corresponding diastolic stage labels. The mean diamonds are shown for each stage, with the center representing the group mean and the top and bottom points represent the 95% confidence intervals. Similarly, the box and whisker plots shown, the center line within the rectangle represents the group median value, the top and bottom lines creating the rectangle are the 75% and 25% percentiles respectively.

Analysis using Automated Algorithm

A newly developed automated algorithm was used to analyze the CMM images of the patients included in this study. The detailed development of this algorithm is described in Chapter 1. The algorithm analyzes CMM images in Matlab where a region of interest and the velocity color bar are manually selected from the original image. The color scale is analyzed for its red, green, and blue color values and a cubic-spline is fit in order to create a quantitative velocity-color scale. Image processing techniques are used to remove grey background noise and the color scale cubic-spline values are then used to create a point-by-point velocity reconstruction of the remaining image. This is a necessary step because the raw velocity data is unavailable and must be recreated from archived images. These steps are shown for a representative patient in Figure 2.1A-C.

A de-aliasing technique similar to the techniques used by Thomas et al. and Rovner et al. [20, 21] was used to reconstruct the image shown in Figure 2.1D.

The reconstructed de-aliased velocity fields, also shown in Figure 2.1D, are also used to calculate the pressure fields by integrating the Navier-Stokes equation assuming one-dimensional incompressible flow:

$$\frac{\partial p}{\partial s} = -\rho\left(\frac{\partial v}{\partial t} + v\frac{\partial v}{\partial s}\right) + \mu\frac{\partial^2 v}{\partial s^2} \qquad 2.1$$

This equation calculates a pressure gradient as the sum of the acceleration and viscous terms, where P is the pressure, ρ is a constant density, u is the velocity vector, t is the time, and μ is a constant dynamic viscosity. The pressure difference between two points along the same CMM scanline can be calculated as a line integral between them. The entire pressure field relative to the ROI mitral valve tip location is calculated integrating to each point along a single scanline [22]. The velocity values measured by the CMM along the scanline are one-dimensional velocities extracted from a three-dimensional flow field; therefore the magnitude of these velocities may be incorrect because no out of plane velocities are captured. The inaccuracy of the velocity measurements will be propagated to the calculated relative pressures.

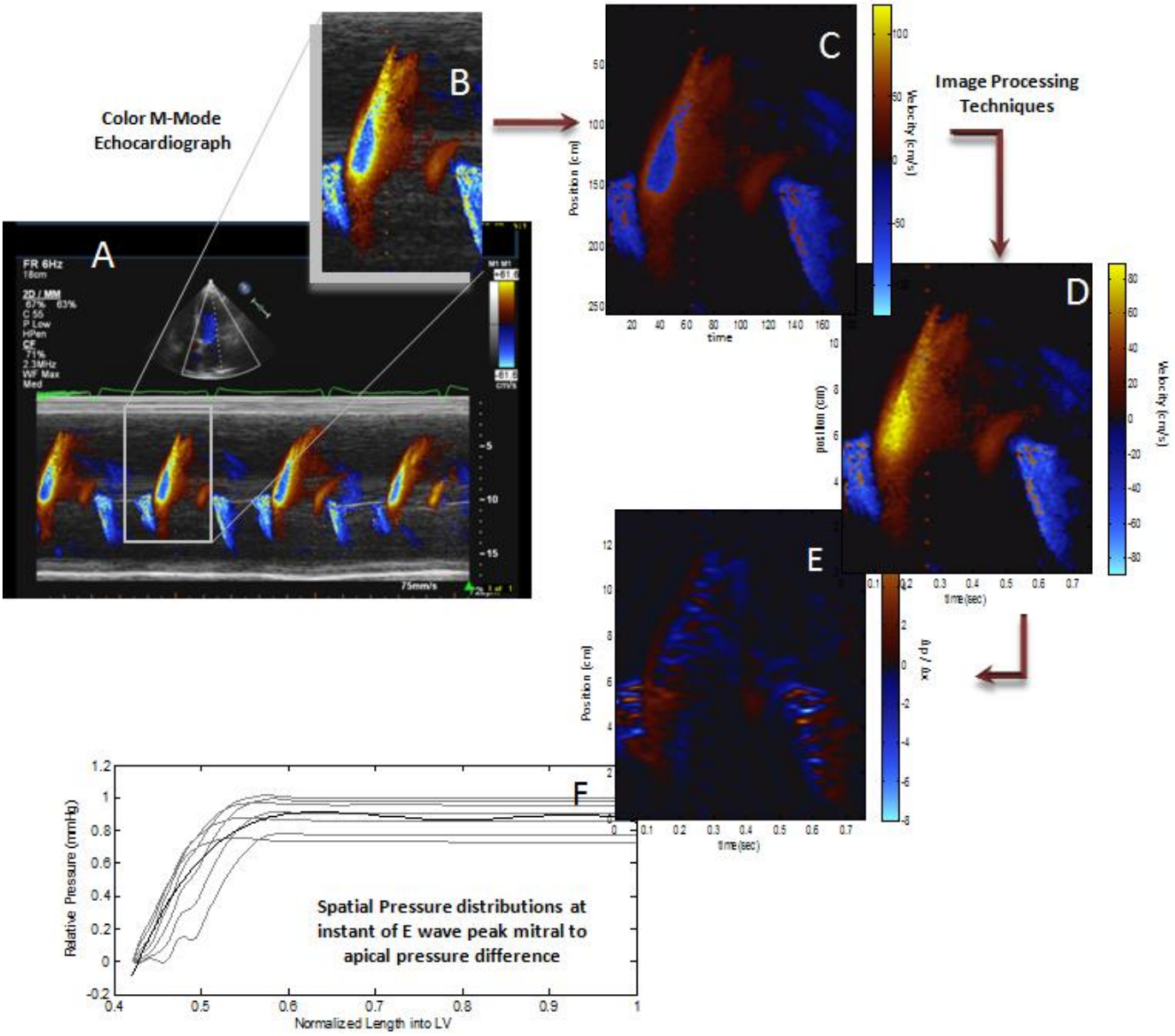

Figure 2.1: Color M-Mode Region of Interest of a Stage 3 restrictive filling patient displaying anti-aliasing techniques

Once the pressure field is reconstructed, instantaneous pressure distributions along a scanline are analyzed. The change in pressure with respect to space, $\Delta p/\Delta x$ is plotted in Figure 2.1E. The pressure difference from the mitral valve to the apex is then calculated and used to determine the instants of maximum ΔP for both the E and A waves. Once the time of the E wave peak pressure difference (PPD) from the mitral valve to the atrium is determined which is indicated in Figure 2.2, the spatial pressure waveform can be resolved. The spatial pressure waveform is the pressure at a single time instant, relative to the mitral valve tip pressure at each position along a line from the mitral valve tips to the apex. A series of seven spatial pressure waveforms are generated at the time-steps centered on the time of the PPD as shown in Figure 2.1F.

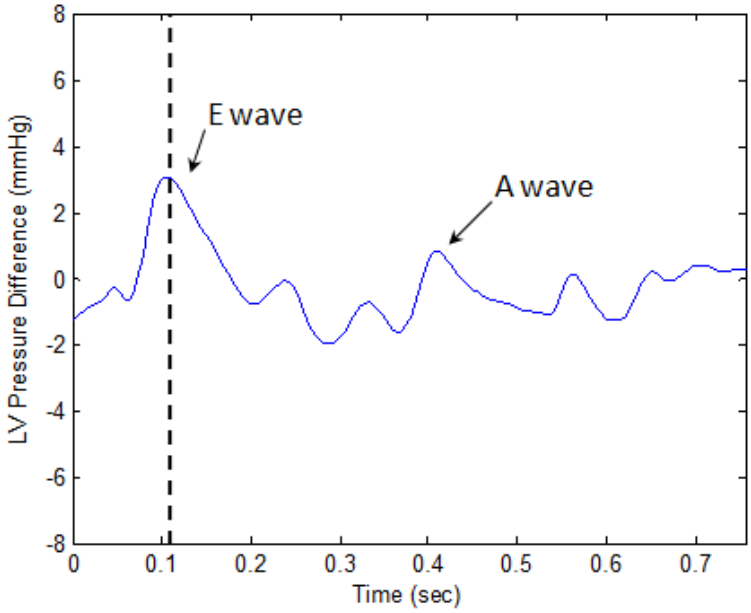

Figure 2.2: Mitral to apex pressure difference (mmHg)

Ensemble Contour Methodology

Due to errors inherent in the acquisition process a single spatial pressure distribution contour will contain noise or artifacts that may produce a spatial pressure distribution estimate that is not characteristic of the filling wave. In this analysis, a series of contours is used to statistically reconstruct an ensemble contour to eliminate the noise or artifacts associated with individual waveforms. Error analysis of 25 representative patients spanning the five categories considered in this study revealed using a minimum of seven spatial pressure waveforms provides an optimal numbers for the ensemble contour reconstructions. This ensures that in all representative cases there was no more than a 1% change in r^2 values with an increasing number of waveforms. For the spatial pressures a series of spatial waveforms was created for each patient. A 2^{nd} , 3^{rd}, and 4^{th} order polynomial are sequentially fit to the series of waveforms. The best fit is selected based on the polynomial with the highest coefficient of determination. The polynomial with the best fit is used in the subsequent analysis to describe the ensemble contour. Figure 2.3 displays the seven spatial pressure contours and the ensemble spatial pressure contour plotted in bold. The spatial pressures are plotted as a relative pressure at a distance into the LV normalized by the total LV length.

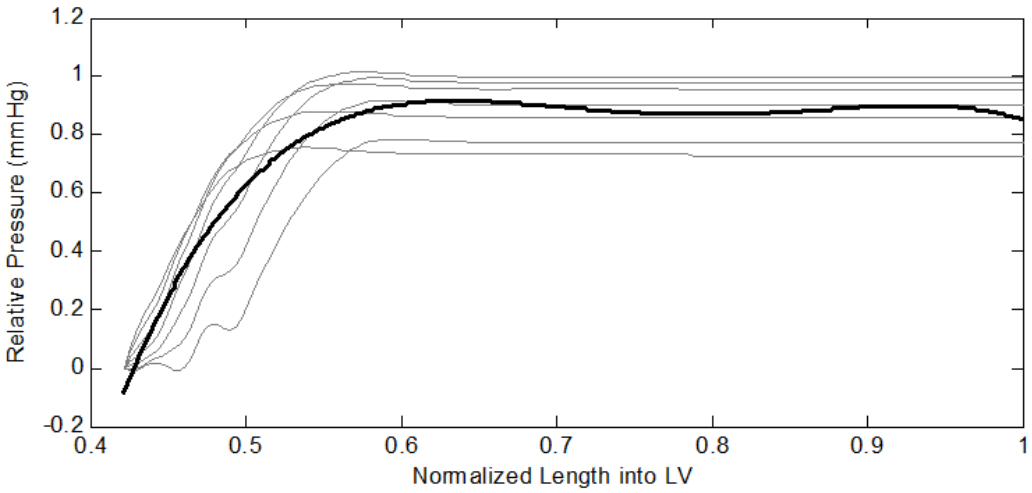

Figure 2.3: Spatial pressure distribution contours with the ensemble contour shown in bold

Change-Point Methodology

Preliminary analysis of the spatial pressure waveforms revealed the consistent presence of a discontinuity point within the spatial waveform. Most often after this initial break point, the slope was reduced or slowly decreased. In an effort to explore the physical significance of this variation, an algorithm was developed to deliver reliable and consistent estimation using a statistical change-point analysis that determines the most statistically significant change in the curve slope.

The change-point analysis is a statistical algorithm used to quantify the most statistically significant change along a waveform. The ensemble contours calculated in the Ensemble Contour Methodology section are used as the input waveforms for the change-point analysis. The change-point analysis was used on the ensemble contours to determine the point of the most statistically significant change within the waveform. The method is based on a cumulative sum of the difference between the value of interest, x_i, and the mean value, $\bar{x}$. Equation 2.2 displays the cumulative sum equation

$$CumulativeSum_i = CumulativeSum_{i-1} + (x_i - \bar{x}) \qquad 2.2$$

The waveform produced by the output of the cumulative sum equation is then plotted to determine the significance of change throughout the signal [23, 24]. The peaks within this cumulative sum waveform are found and sorted according to their magnitude. The peak with the highest magnitude signifies the most statistically significant change. Any number of feasible change-points can be calculated and sorted based on significance using this method. In this work a single change-point, corresponding to the most statistically significant change is utilized. The most statistically significant change in the waveform is labeled as the critical-point throughout this analysis. The ensemble contours for the spatial pressure ensure that a global change in the waveform is detected as the critical-point. Three representative patient ensemble contours are shown in Figure 2.4 with the location of the critical-point indicated by the dashed line.

Plateau-Point Methodology

Preliminary analysis of the spatial pressure distributions also exposed a second point of interest within the waveforms at which the pressure relative to the mitral valve pressure became reasonably constant. This location will be referred to as the plateau-point and is calculated as the distance into the ventricle at which the pressure plateaus and begins to change by less than 0.25% of the peak pressure for at least 10% of the total length of the LV. The plateau-points for three representative spatial pressure waveforms are shown in Figure 2.4. The majority of waveforms remain at a relatively constant pressure after the plateau-point, but a small percentage of patients show slight variations in the pressure past the plateau-point as demonstrated in Figure 2.4C.

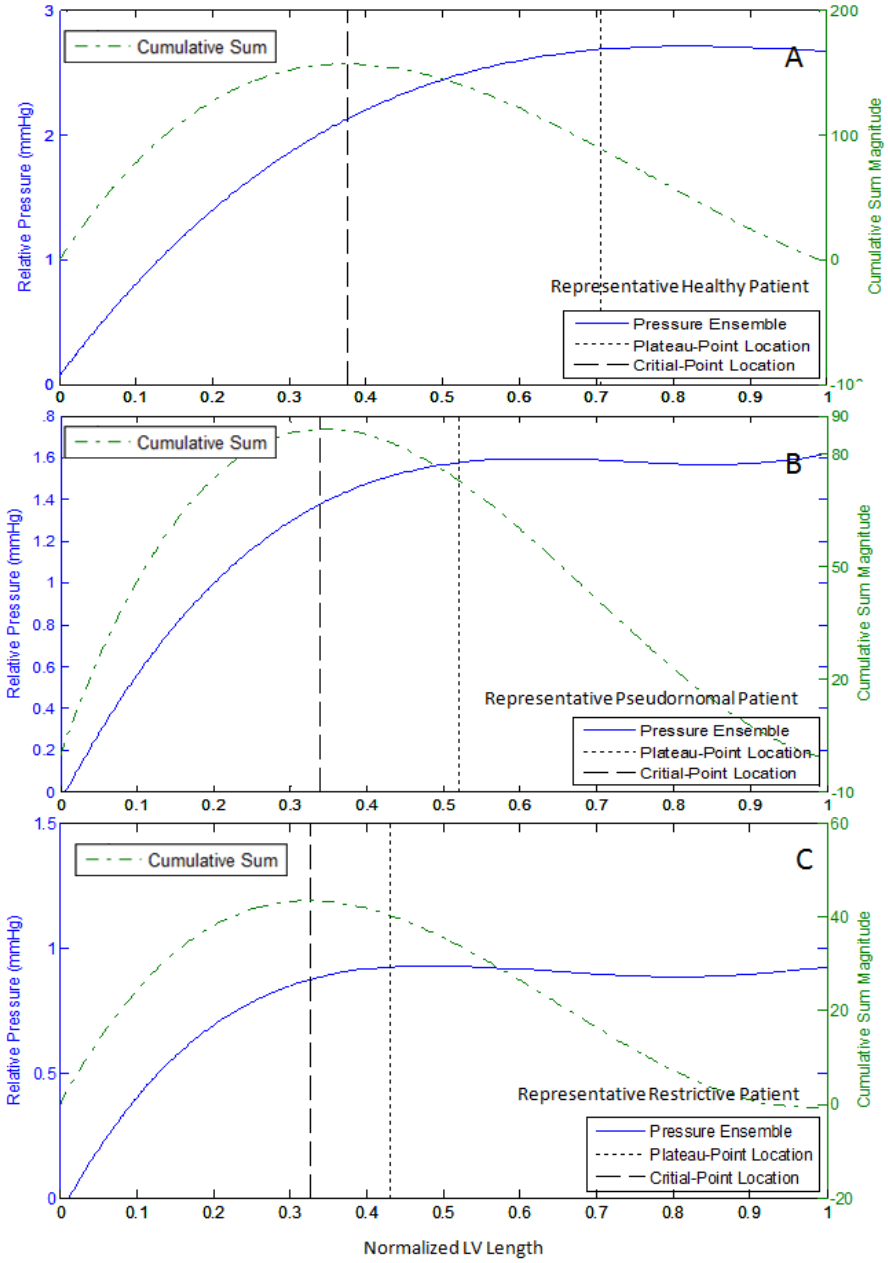

Figure 2.4: Three representative spatial pressure ensemble contours, showing critical-point location, plateau-point location, and corresponding cumulative sum contours

Results

There has been relatively little emphasis on the changes in pressure with respect to the length of the LV towards the understanding of diastolic dysfunction. Analyzing the spatial pressure distributions can uncover critical-points within the filling wave that have previously been undetected. The spatial pressure distributions discussed in the pressure calculation methodology section of Chapter 1 are statistically analyzed to calculate the mean and median waveforms for each category shown in Figure 2.5.

The waveforms shown are the calculated mean and median spatial pressure waveforms per category where the mean and median pressure magnitudes are calculated at each normalized location of the LV, which is the distance into the LV divided by total LV length. The x-axis represents the distance into the LV, x, normalized by the total LV length shown in equation 2.3:

$$Normalized\ LV\ Length = \frac{x}{L_{LV}} \tag{2.3}$$

The waveforms exhibit an overall decrease in magnitude and therefore a decline in peak mitral to apical pressure difference as diastolic function decreases. The analysis of the spatial pressure waveforms is adapted from the analysis performed by Yotti et al.'s study of dilated cardiomyopathy patients [7]. This type of analysis has never before been performed on diastolic dysfunction patients.

In Figure 2.5, the mean curves excessively smooth the spatial waveform and are believed to be less representative of the spatial pressure values within the LV than the median. The median curves display noticeable changes in the waveform slope throughout the length of the LV.

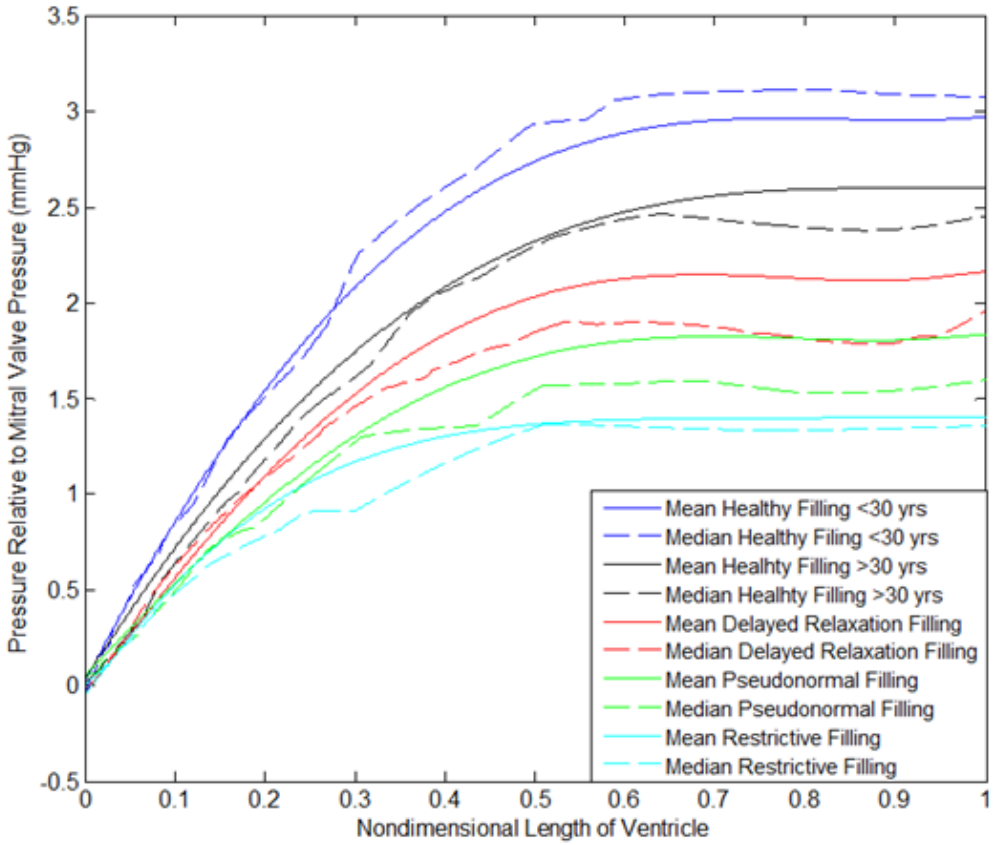

Figure 2.5: Spatial Pressure Distribution at Peak Mitral to Apical Pressure Difference during Early Diastole

The pressure critical-point location for each patient is plotted in Figure 2.6A as calculated in the change-point methodology section. In this variability plot the centerline of each diamond indicates the group mean value and the top and bottom apex of the triangle show the 95% confidence interval of the mean. The width of each triangle is related to the number of samples in each group. The centerline of the box and whisker rectangle indicates the median value for each group and the top and bottom lines of the rectangle display the 25^{th} and 75^{th} percentile values. The horizontal bars on the top of the image shows the groups with statistically different mean values. The y-axis is the distance into the LV past the mitral valve tips normalized by the total length of the ventricle. As shown in the spatial pressure distribution plot, the normalized distance into the ventricle at which the critical-point occurs slightly decreases as the diastolic dysfunction classification worsens from 35.3 ± 4.5 % of the distance into the LV for healthy patients to 26.2 ± 7.7% for restrictive filling patients. The healthy patients are not statistically significant from the mildly diseased stages, delayed relaxation and psedonormal filling and there is very little change overall in the normalized location of the critical-point.

The normalized plateau-point location is plotted by diastolic dysfunction stage in Figure 2.6B. The normalized plateau-point location is the location at which the plateau-point occurs, as described in the plateau-point methodology section, normalized by the total length of the LV. The mean plateau-point for the healthy patients is 68.2 ± 8.0% and 48.4 ± 11.3% for restrictive filling patients. Both healthy categories are statistically different from all three diseased categories, indicating that there is an inverse correlation between diastolic dysfunction stage and plateau-point location. The healthy patients reach a plateau later than the diseased cases, allowing the positive pressure gradient to extend further into the LV. This can be associated with a stronger and more effective early filling wave of the healthy patients relative to the severely diseased patients.

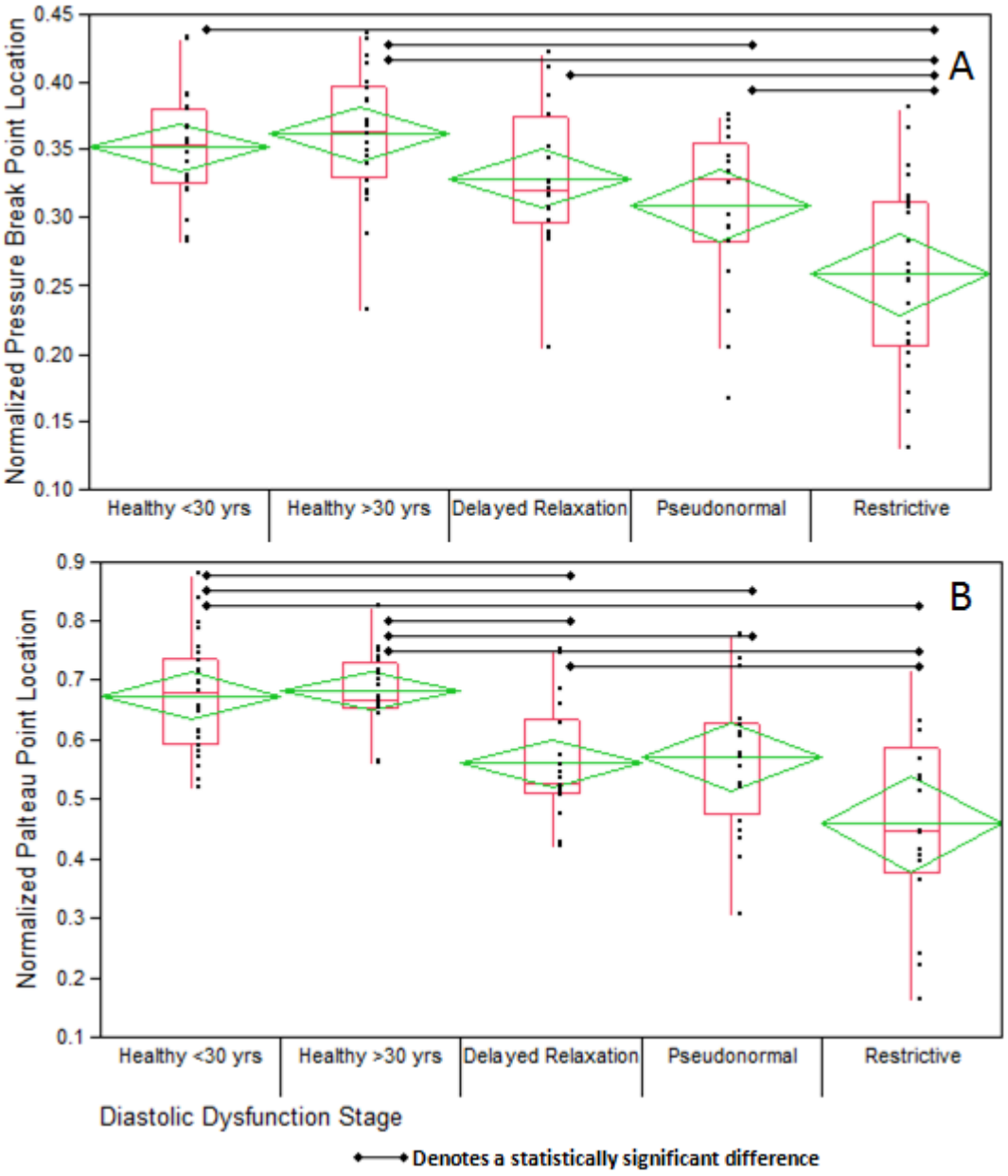

Figure 2.6: Normalized Pressure Critical-point Location and Normalized Pressure Plateau-point Location

The pressures at both the location of the critical-point and the location of the plateau-point of the spatial pressure waveform are calculated and the ratio of these pressures is displayed in Figure 2.7. The critical-point pressure and plateau-point pressure have a smaller ratio for healthier patients than for severely diseased patients. The mean healthy pressure at the critical-point is 76.1 ± 5.1% of the plateau pressure and the mean restrictive pressure at the critical-point is 82.2 ± 5.0% of the plateau-point. This

change in pressure ratios indicates that there is a larger rise in pressure between the two points of interest for healthy patients.

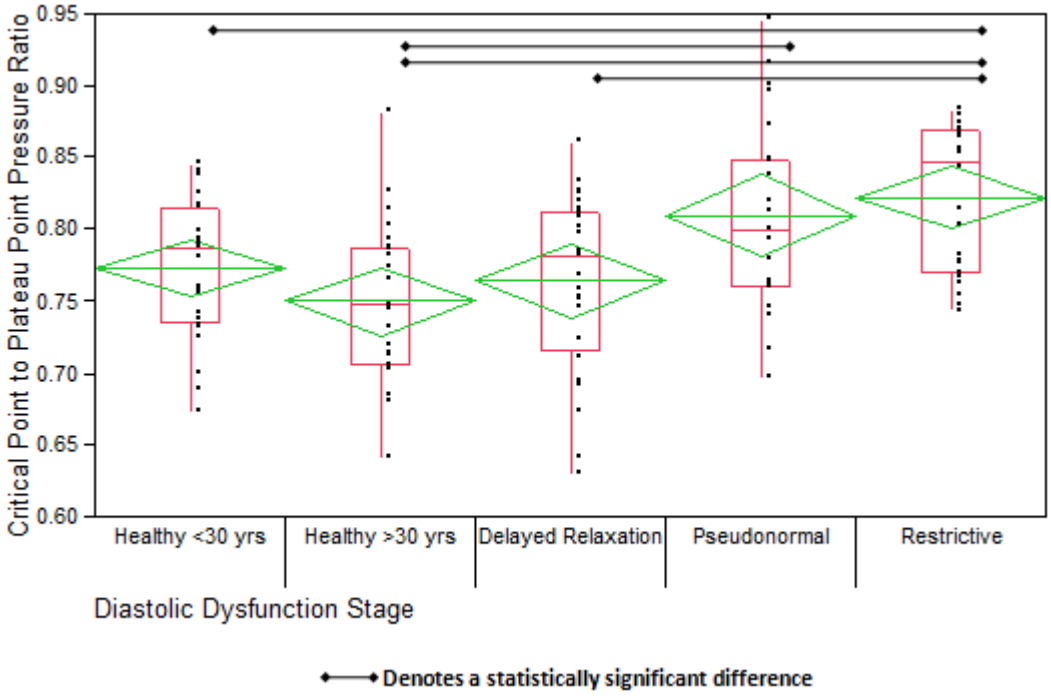

Figure 2.7: Critical-point Pressure Ratio and Normalized Pressure Plateau Position

The normalized locations for the two points of interest, the critical-point and the plateau-point, are compared in Figure 2.8. The y-axis is the distance into the LV normalized by the total length of the ventricle. The x-axis is labeled by diastolic dysfunction stage where each vertical color line represents a single patient in the study. In this plot the mitral to apical peak pressure difference can be seen from the pressure magnitudes along the top of the figure with the peak pressure decreasing as the diastolic dysfunction stage increases. The black circles indicate the normalized location of the critical pressure point for each patient and the black stars show the normalized location of the plateau-point. The least squares lines tracking the decrease in critical-point and plateau-point location are solely to aid in the visual analysis of the decline with respect to diastolic dysfunction stage and not to indicate a continuous relationship between individual patients within each stage. The plateau-point location is decreasing much faster with decreasing diastolic dysfunction stage than the critical-point location showing that the two points of interest are closer together for diseased patients than healthy patients.

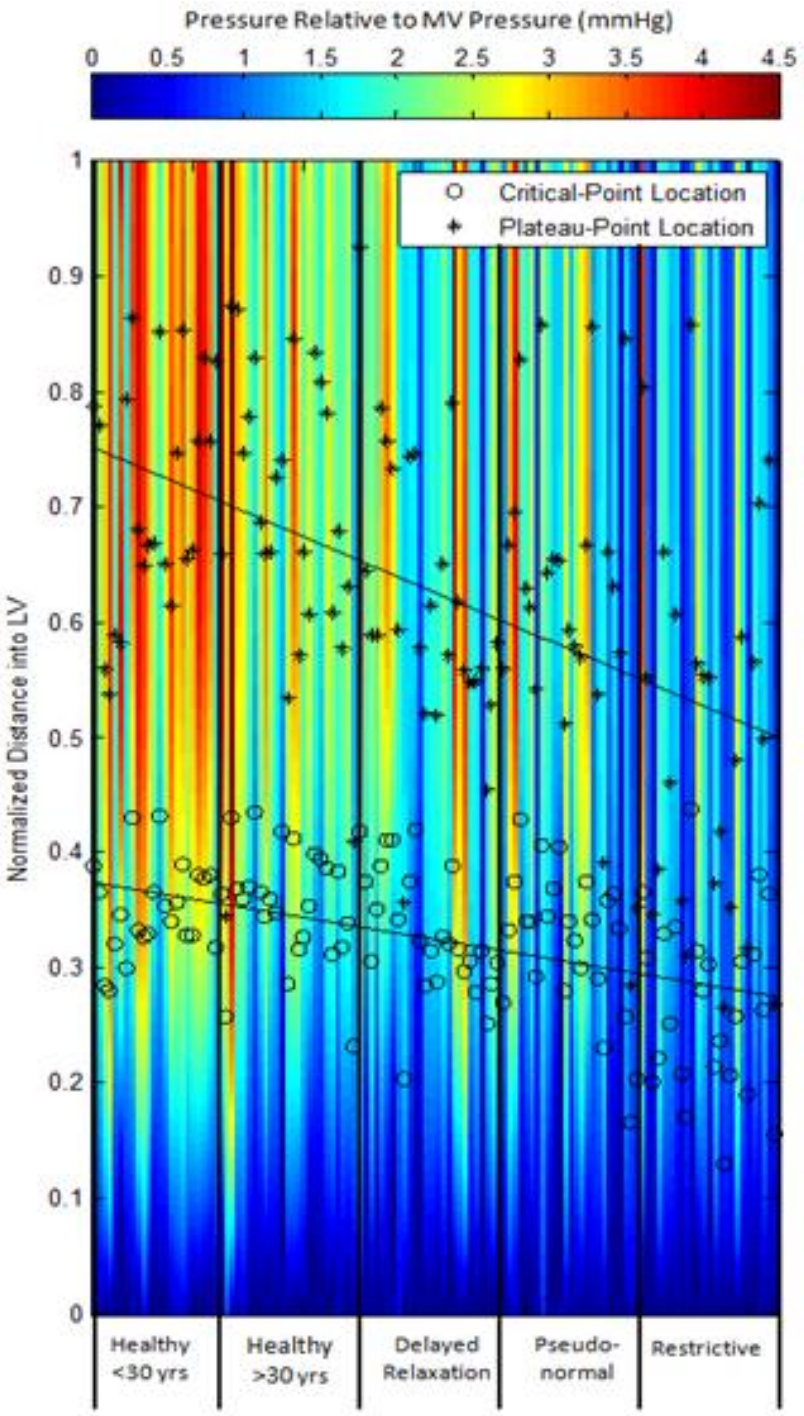

Figure 2.8: Comparison of Critical-point Location and Plateau-point Location

The quantification of the two specific locations within the filling pressure wave dissects the waveform into three regions as shown in Figure 2.4 and Figure 2.8. The first region is the initial filling wave which occurs from the onset of the E wave to the location of the critical-point and is driven by the early relaxation of the LV. The normalized duration of this region is relatively constant for all stages of diastolic dysfunction with the mean healthy duration being 35.3 ± 4.5 % and the mean restrictive duration being 26.2 ± 7.7% of the LV length as shown in Figure 2.6A. Figure 2.8 displays a subtly declining slope tracking the critical-point locations, from this and the lack of statistical significance shown in Figure 2.6A it is assumed that there is little dependence on the diastolic function of the LV for the rapid initial relaxation initiating the E wave.

The second region, occurring between the critical-point location and the plateau-point location is the region of secondary filling. The normalized distance to the end of this region ranges from 68.2 ± 8.0% for healthy patients to 48.4 ± 11.3% for restrictive filling cases as shown in Figure 2.6B. In addition to the length reduction of this region with decreasing diastolic function, the pressure increase during this region lessens. The critical-point to plateau-point pressure ratio for healthy patients is 75.2 ± 4.5% and increases to 82.5 ± 4.8% for restrictive cases, displayed in Figure 2.7. The change in duration of this region and pressure changes within the region are due to a reduction in relaxation of the LV. The healthy patients reach the spatial pressure critical-point and the gradient slowly changes until it reaches it plateauing pressure. In the severely diseased patients, the spatial pressure critical-point is reached and the pressure stops at the plateauing pressure more abruptly. This abrupt change during the useful filling phase can be attributed to the onset of the strong decline in the favorable pressure gradient. The healthy patients do not exhibit a drastic decline in the favorable pressure gradient which allows the spatial pressure waveforms to smoothly reach their plateauing pressure. The combination of the initial filling region and the secondary filling region are combined to make-up the useful filling of the E wave.

The third region is the constant pressure region, this occurs after the plateau-point where the pressure relative to the mitral valve pressure is relatively constant. There is no pressure gradient and therefore this is a region of inertial filling.

Discussion

The current study demonstrates previously unexplored characteristics of the LV spatial pressure distribution which are directly linked to the efficiency of early diastolic filling. A noninvasive calculation of the spatial pressure distribution at the instant of peak mitral to apical pressure difference during the E wave was used to characterize the region of initial filling, secondary filling, and constant pressure filling. The pressures and normalized lengths into the LV at the two points of interest, the critical-point and plateau-point locations, are compared to determine how the useful filling area changed as a result of the diastolic function.

The length of the initial filling region is relatively constant for all stages of diastolic dysfunction with the mean values changing only 8% from healthy to restrictive filling patients. This region is linked to the initial columnar flow into the LV at the instant of the mitral valve opens [25]. Past this initial columnar motion, the pressure wave is affected by the properties of the LV such as amount of relaxation and compliance. A healthy LV relaxes during early diastole and continuously sucks blood towards the apex. This filling process creates a progressive pressure gradient for the majority of the length of the LV. In the secondary filling region of the spatial pressure waveform the pressure smoothly increases until the plateau pressure is reached at 68.2 ± 8.0 % of the total LV length. The pressure at the critical-point is only 75.2 ± 4.5% of the plateau pressure allowing the pressure to rise an average of 25% of the total pressure within the useful filling region. In the severe stages of diastolic dysfunction, the relaxation of the ventricle is drastically reduced causing the atrial pressure to increase. In these cases the blood is forced into the ventricle during the early filling by the increased atrial pressure. The combination of the decline in left ventricular relaxation, decreased LV compliance, and the increased left atrial pressure

causes the incoming blood to be subjected to a strong decline in the favorable pressure gradient closer to the mitral valve. The LV is not enlarging at a healthy rate causing the blood within the ventricle to be relatively stagnant and create an opposition for the incoming flow. The secondary filling region is shortened in the diseased cases forcing the plateau-point location to occur at only 48.4 ± 11.3% of the total length of the LV. The decrease in the length of the secondary filling region is correlated with a decreased change in pressures over this region; the ratio of critical-point to plateau-point pressure is 82.5 ± 4.8%. The constant pressure region is the remainder of the filling to the apex of the LV after the completion of the useful filling region. This section of the flow is no longer pressure driven flow but is inertial driven flow.

The duration of the secondary filling region can be linked to the mechanism driving the E wave filling and therefore the efficiency of the filling. Healthy patients are a purely suction driven filling, caused by LV relaxation, and therefore have a longer secondary filling region. Severely diseased patients have the E wave blood flow forced into the LV from the higher pressures in the atrium [6]. The pressure gradient forcing blood into the LV generated by the high pressure atrium is more rapidly decreased because LV relaxation and LV compliance are reduced. The patients between healthy and severely diseased have a combination of both LV suction and high atrial pressures driving the E wave and therefore these patients have a useful filling region duration between healthy and diseased.

The efficiency of the early filling wave can be calculated using the instantaneous spatial pressure waveform. The integral of the waveform times the length of the LV represents the total work per unit area of the E wave referred to as W_{Total} shown in Figure 2.9. Similarly, the work per unit area of the total useful work per unit area, including the initial and secondary regions is calculated as W_{useful}. After calculating the useful work per unit area and the total work per unit area, a Useful Filling Efficiency can be calculated in equation 2.4:

$$\eta_{UsefulEfficiency} = \frac{W_{Useful}}{W_{Total}} \qquad 2.4$$

This equation represents a true efficiency of useful work divided by total work of the E wave. The area component in the work per unit area terms W_{Useful} and W_{Total} are canceled when the values are divided by one-another. The initial filling region stays fairly constant; therefore the secondary filling region represents the change in valuable work as the diastolic function of the LV decreases. The useful filling efficiency parameter is plotted in Figure 2.10. The healthy filling patients have a mean useful work of 64.8 ± 12.7% of the total work of the E wave and the useful of the restrictive patients falls to 37.1 ± 12.1%.

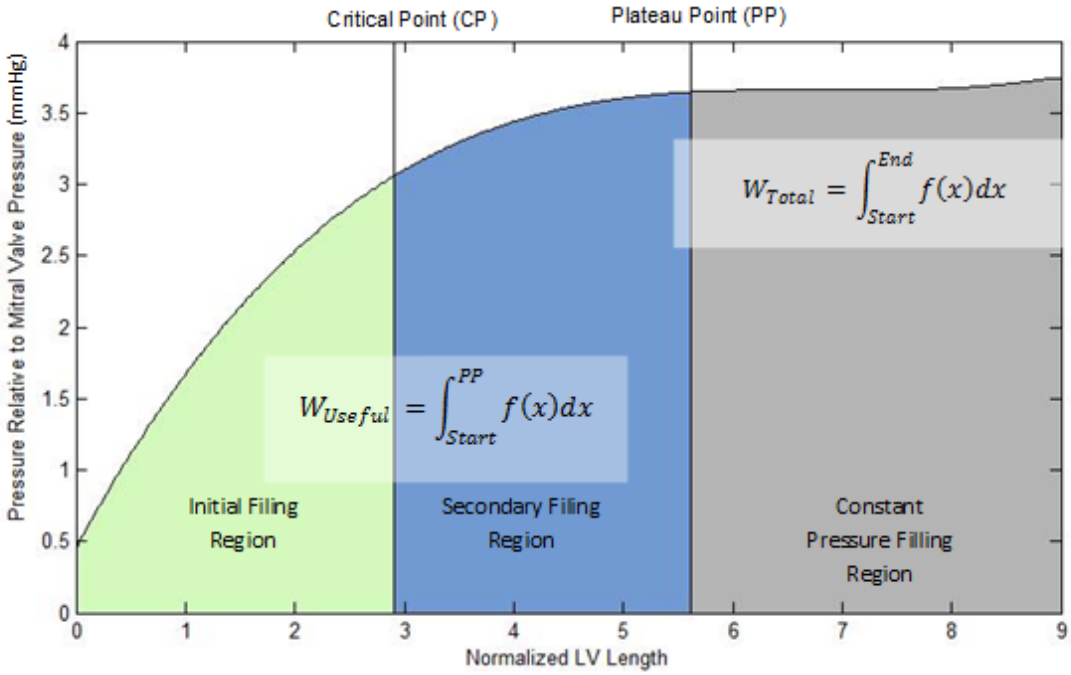

Figure 2.9: Representative spatial pressure waveform indicating initial, secondary and constant pressure filling regions and the work per unit area integrals for each region. The spatial pressure waveform is represented by f(x).

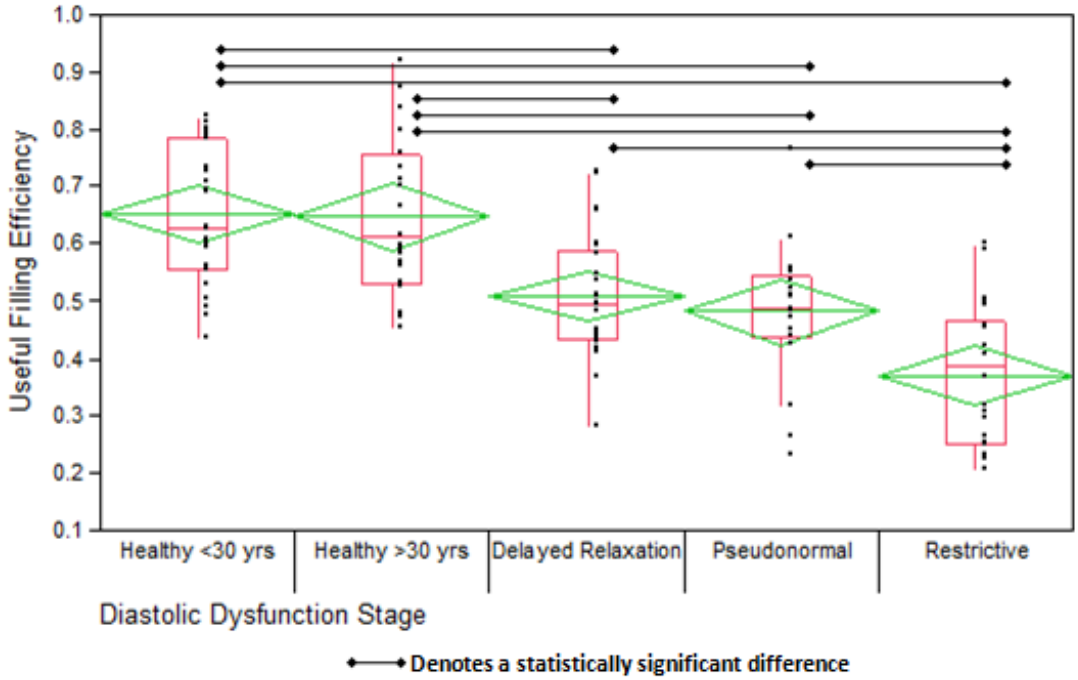

Figure 2.10: Useful filling efficiency calculated from ensemble pressure waveforms

The length and pressure changes of the useful filling region are employed to calculate the change in the work per unit area of the useful filling region as the diastolic function worsens. The changes in the location of the plateau-point and the change in pressure during the useful filling region are related to the strength and location of the rate of decline in the pressure gradient driving the flow and therefore are correlated with the E wave filling efficiency. Future work involving BNP and clinical diastolic dysfunction survival studies should be completed to verify the correlations shown in this analysis.

Conclusions

A spatial pressure analysis was performed on Color M-Mode echocardiography images and a novel filling efficiency was introduced. The pressure distribution within the LV during early filling is an important parameter to understanding the decline of diastolic dysfunction but the spatial pressure distribution at the time of peak mitral to apical pressure difference has never before been examined in patients with diastolic dysfunction. From this analysis, three regions of filling were defined which aid in the characterization and understanding of healthy and diseased early filling waves. The initial filing region, driven by the initial left ventricular relaxation of the E wave, is relatively disease independent and its duration ranges from 35.3 ± 4.5 % of the total left ventricular length for healthy patients to 26.2 ± 7.7% of total left ventricular length for restrictive filling patients. The secondary filling region is located between the critical-point and the plateau-point of the spatial pressure waveform and is the site of the majority of distinction between healthy and diseased filling. Healthy patients have a larger spatial distance between the critical-point and plateau-point that diseased filling patients allowing for a greater pressure increase in the secondary filling region. The duration of the secondary declines as the ventricle changes from a healthy relaxation driven early filling to a diseased left atrial pressure driven filling. The decline in efficiency is calculated as the filling mechanism changes and the useful filling region decreases. Healthy patients have a useful filling efficiency of 64.8 ± 12.7% and the useful filling efficiency of restrictive filling patients drops to 37.1 ± 12.1%.

References

1. Brun, P., et al., *LEFT-VENTRICULAR FLOW PROPAGATION DURING EARLY FILLING IS RELATED TO WALL RELAXATION - A COLOR M-MODE DOPPLER ANALYSIS.* Journal of the American College of Cardiology, 1992. **20**(2): p. 420-432.
2. Garcia, M.J., J.D. Thomas, and A.L. Klein, *New Doppler echocardiographic applications for the study of diastolic function.* Journal of the American College of Cardiology, 1998. **32**(4): p. 865-875.
3. Oh, J.K., *Echocardiography in heart failure: Beyond diagnosis.* European Journal of Echocardiography, 2007. **8**(1): p. 4-14.
4. Quinones, M.A., *Assessment of diastolic function.* Progress in Cardiovascular Diseases, 2005. **47**(5): p. 340-355.
5. Vandervoort, P.M., et al. *ESTIMATION OF LEFT-VENTRICULAR FILLING GRADIENTS USING DIGITAL ANALYSIS OF COLOR DOPPLER M-MODE-VELOCITIES*. in *20th Annual Meeting of Computers in Cardiology*. 1993. London, England.
6. Claessens, T.E., et al., *New echocardiographic applications for assessing global left ventricular diastolic function.* Ultrasound in Medicine and Biology, 2007. **33**(6): p. 823-841.
7. Yotti, R., et al., *A noninvasive method for assessing impaired diastolic suction in patients with dilated cardiomyopathy.* Circulation, 2005. **112**(19): p. 2921-2929.
8. Greenberg, N.L., et al. *Significance of color Doppler M-mode scanline orientation in the non-invasive assessment of intraventricular pressure gradients*. in *24th Annual Computers in Cardiology Conference*. 1997. Lund, Sweden.
9. Rovner, A., et al., *Characterization of left ventricular diastolic function in hypertension by use of Doppler tissue imaging and color M-mode techniques.* Journal of the American Society of Echocardiography, 2006. **19**(7): p. 872-879.
10. Khouri, S.J., et al., *A practical approach to the echocardiographic evaluation of diastolic function.* Journal of the American Society of Echocardiography, 2004. **17**(3): p. 290-297.
11. Lew, W.Y.W., *EVALUATION OF LEFT-VENTRICULAR DIASTOLIC FUNCTION.* Circulation, 1989. **79**(6): p. 1393-1397.
12. Dorosz, J.L., K.G. Lehmann, and J.R. Stratton, *Comparison of tissue Doppler and propagation velocity to invasive measures for measuring left ventricular filling pressures.* American Journal of Cardiology, 2005. **95**(8): p. 1017-1020.
13. Little, W.C., *Diastolic dysfunction beyond distensibility - Adverse effects of ventricular dilatation.* Circulation, 2005. **112**(19): p. 2888-2890.
14. Greenberg, N.L., et al., *Estimation of diastolic intraventricular pressure gradients by Doppler M-mode echocardiography.* American Journal of Physiology-Heart and Circulatory Physiology, 2001. **280**(6): p. H2507-H2515.
15. Rovner, A., et al., *Relationship of diastolic intraventricular pressure gradients and aerobic capacity in patients with diastolic heart failure.* American Journal of Physiology-Heart and Circulatory Physiology, 2005. **289**(5): p. H2081-H2088.
16. Popovic, Z.B., et al., *Relationship among diastolic intraventricular pressure gradients, relaxation, and preload: impact of age and fitness.* American Journal of Physiology-Heart and Circulatory Physiology, 2006. **290**(4): p. H1454-H1459.
17. Thomas, J.D. and Z.B. Popovic, *Intraventricular pressure differences - A new window into cardiac function.* Circulation, 2005. **112**(12): p. 1684-1686.
18. Smiseth, O.A., et al., *Mechanics of intraventricular filling: study of LV early diastolic pressure gradients and flow velocities.* American Journal of Physiology-Heart and Circulatory Physiology, 1998. **44**(3): p. H1062-H1069.

19. Hunt, S.A., et al., *ACC/AHA guidelines for the evaluation and management of chronic heart failure in the adult: Executive summary - A report of the American College of Cardiology/American Heart Association Task Force on Practice Guidelines (Committee to Revise the 1995 Guidelines for the Evaluation and Management of Heart Failure).* Journal of Heart and Lung Transplantation, 2002. **21**(2): p. 189-203.
20. Thomas, J.D., et al. *DIGITAL ANALYSIS OF TRANSMITRAL COLOR DOPPLER M-MODE DATA - A POTENTIAL NEW APPROACH TO THE NONINVASIVE ASSESSMENT OF DIASTOLIC FUNCTION*. in *Conf on Computers in Cardiology*. 1992. Durham, Nc.
21. Rovner, A., et al. *Improvement in diastolic intraventricular pressure gradients in patients with HOCM after ethanol septal reduction*. in *Annual Meeting of the American-College-of-Cardiology*. 2002. Atlanta, Georgia.
22. Charonko, J.J., P.P. Vlachos, and Asme. *Keynote paper: Time-accurate measurement of pressure from particle image velocimetry data*. in *5th Joint ASME/JSME Fluids Engineering Summer Conference*. 2007. San Diego, CA.
23. Taylor, W.A., *Change-Point Analysis: A Powerful New Tool For Detecting Changes*. 2000.
24. Hinkley, D.V., *Inference about the Change-Point from Cumulative Sum Tests* Biometrika 1971. **58**(3): p. 509-523
25. De Boeck, B.W.L., et al., *Colour M-mode velocity propagation: a glance at intra-ventricular pressure gradients and early diastolic ventricular performance.* European Journal of Heart Failure, 2005. **7**(1): p. 19-28.

Overall Conclusion

This work introduces a newly developed automated algorithm for the analysis of color M-moe echocardiography data as well as an indepth analysis of the early filling wave velocities and spatial pressure distributions as left ventricular diastolic function declines. The velocity critical point analysis quantifies a point of deceleration within the early filling wave velocity which has been previously observed but never before analyzed. Through the calculation of this parameter, a new method of analyzing eary filling wave velocities is introduced and the length of the critical point and the critial propagation velocity is calcualted with an increased inverse correlation with declining diastolic function. The pressure analysis completed views the spatial pressure distributions along the length of the left ventricle from the mitral valve to the apex for the first time for patients with varying stages of diastolic dysfunction. Both the magnitude of the waveform and the shape of the waveform were analyzed displaying a decline in the peak mitral to apical difference from healhty to diseased patients as well as a change in the overall waveform shape as diastolic function declines. By splitting the pressure waveforms into three sections, it was determined that the secondary filling region is most effected by changes in the LV filling. The duration of the secondary region declines as the ventricle changes from a healthy relaxation driven early filling to a diseased left atrial pressure driven filling. The decline in efficiency is calculated as the filling mechanism changes and the useful filling region decreases. Healthy patients have a useful filling efficiency of 64.8 ± 12.7% and the useful filling efficiency of restrictive filling patients drops to 37.1 ± 12.1%.

The velocity and pressure analysis within this work aim to support the hypothesis of a change in the mechanism diring early diastolic filling from a healhty relaxation driven filling to a severely diseased high left atrial pressure driven filling. The decline in the length into the ventricle at which the critial point occurs as well as the decline in the length into the ventricle at which the pressure critial point occurs support this hypothesis by suggesting that the initialy high filling wave velocity is decelerated earlier into the left ventricle and the positive pressure gradient driving early diastole is broken down sooner into the ventricle for diseased patients than for healhty patients. The severely diseased patients therefore have a less efficient early diastolic filling wave due to the decreased early relaxation and increased left ventricular stiffness.

3. Appendix

Appendix A: Error Analysis

Algorithm Component Error Analysis

Velocity Reconstruction

In order for the propagation of error throughout the automated algorithm to be estimated, the uncertainty of each measured or calculated component must be determined. When setting up the automated algorithm developed in Matlab to process a new Color M-mode image a few manual inputs must be entered which have an uncertainty associated with them. First the velocity color bar region is manually selected. By incorrectly cropping the velocity color bar an unnecessarily large velocity error may be introduced before the algorithm begins. This error analysis will begin by assuming the entire color bar region is selected and the proper velocity values are transcribed from the original color M-mode image.

To verify the reconstruction of the region of interest velocity field, a reference analytical velocity field was constructed. The image was digitally saved and imported back into Matlab. The same process used for digitally reconstructing the region of interest velocities was used to reconstruct the reference velocity region using the velocity color bar shown in Figure 3.1. From this analysis the reconstruction velocity errors were calculated as the velocity difference between the original. The mean absolute error between the original and reconstructed velocity fields is 1.17 ± 0.58 cm/s.

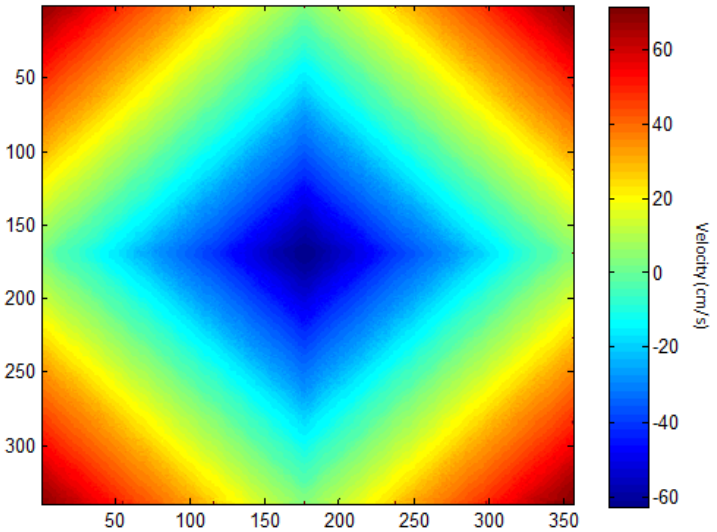

Figure 3.1: Representative Velocity Field

Change-Point Analysis

To verify the accuracy and repeatability of the location chosen by the change-point analysis implemented into the velocity and pressure ensemble waveform analysis two sets of representative contours were created. These contours shown in Figure 3.2 and Figure 3.3 vary from contours with abrupt changes at the location of the change from the initial region to the terminal region to very smooth changes from the initial linear slope to the terminal slope. These waveforms also vary from a terminal region being linear to varying curvature in the terminal region. All transition points are located at 25% of the total length of the waveform in Figure 3.2 and 50% of the total length of the waveform in Figure 3.3. The selection of the critical point using the change-point analysis was calculated on the original waveforms as well as the waveforms with a percentage of white noise added. The results from this study are shown in Table 3.1 for the representative ensemble contours with the break point located at 25% of the total length and Table 3.2 for the representative ensemble contours with the break point located at 50% of the total length.

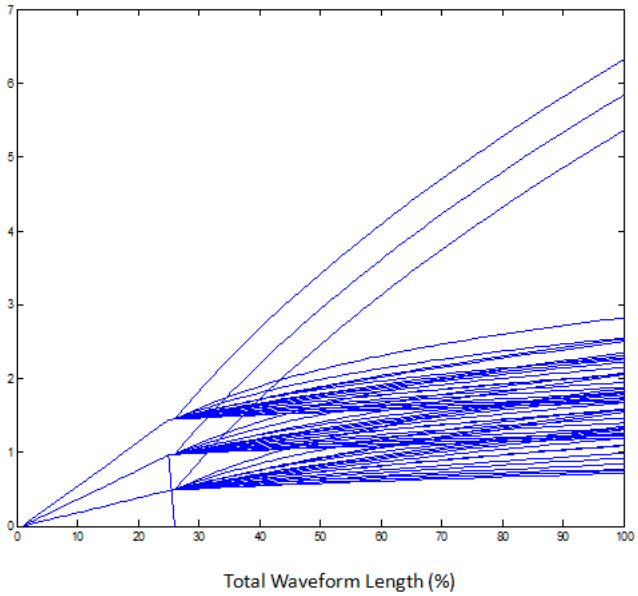

Figure 3.2: Representative ensemble contours with break point at 25% of total length

Table 3.1: Change-Point Analysis Measurements from Representative Ensemble Contours with break point at 25% of total length

White Noise Added	Mean Critical Point (% of total length)	RMS	Bias
0%	23.5	2.2	1.9
1%	23.3	2.5	2.1
5%	22.7	3.4	2.9
10%	22.7	3.5	3.0
15%	22.7	3.6	3.0

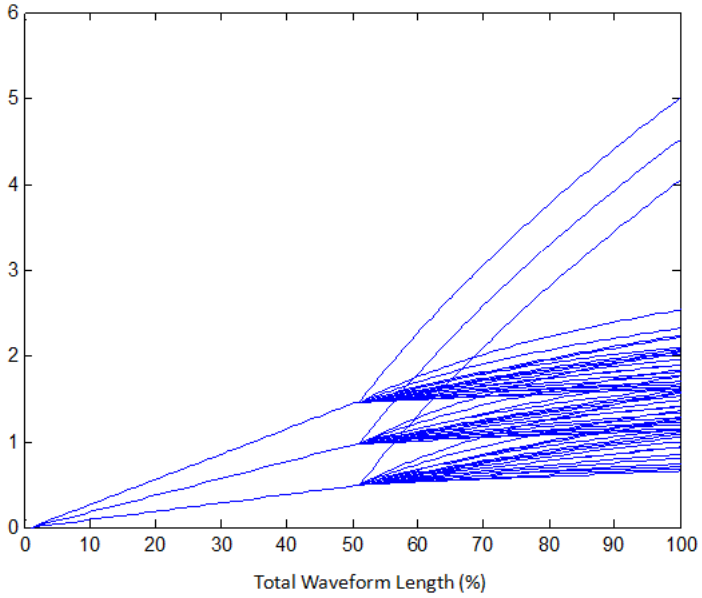

Figure 3.3: Representative ensemble contours with breakpoint at 50% of total length

Table 3.2: Change-Point Analysis Measurements from Representative Ensemble Contours with break point at 50% of total length

White Noise Added	Mean Critical Point (% of total length)	RMS	Bias
0%	47.2	4.1	3.1
1%	47.0	4.0	3.0
5%	47.0	4.2	3.2
10%	47.1	4.2	3.1
15%	47.1	4.1	3.1

Sensitivity Analysis

Basic Equation used in analysis:

$$Vp = \frac{\Delta x}{\Delta t} \tag{3.1}$$

Where Δx is a spatial difference in centimeters and Δt is a temporal difference in seconds.

Associated Error:

$$\delta Vp = \left|\left(\frac{\partial Vp}{\partial \Delta x}\right)\delta\Delta x\right| + \left|\left(\frac{\partial Vp}{\partial \Delta t}\right)\delta\Delta t\right| \tag{3.2}$$

$$\delta Vp = \sqrt{\left(\frac{1}{\Delta t}\right)^2 \delta x^2 + \left(-\frac{\Delta x}{\Delta t^2}\right)^2 \delta t^2} \qquad \textbf{3.3}$$

Where δΔx and δΔt are the errors associated with a spatial or temporal difference and δVp is the error in the calculated relative pressure in mmHg. This error δVp is calculated for each individual pixel change in location and change in time evaluated using average pixel height and duration 0.045cm and 0.0034s. Figure 3.4 displays the error associated with the calculated relative pressure, shown on the x-axis, dependent on the Δt and Δx error independently, shown on the two y-axes. The range of δΔt and δΔx are 0 to half the mean temporal or spatial duration of the pixel respectively.

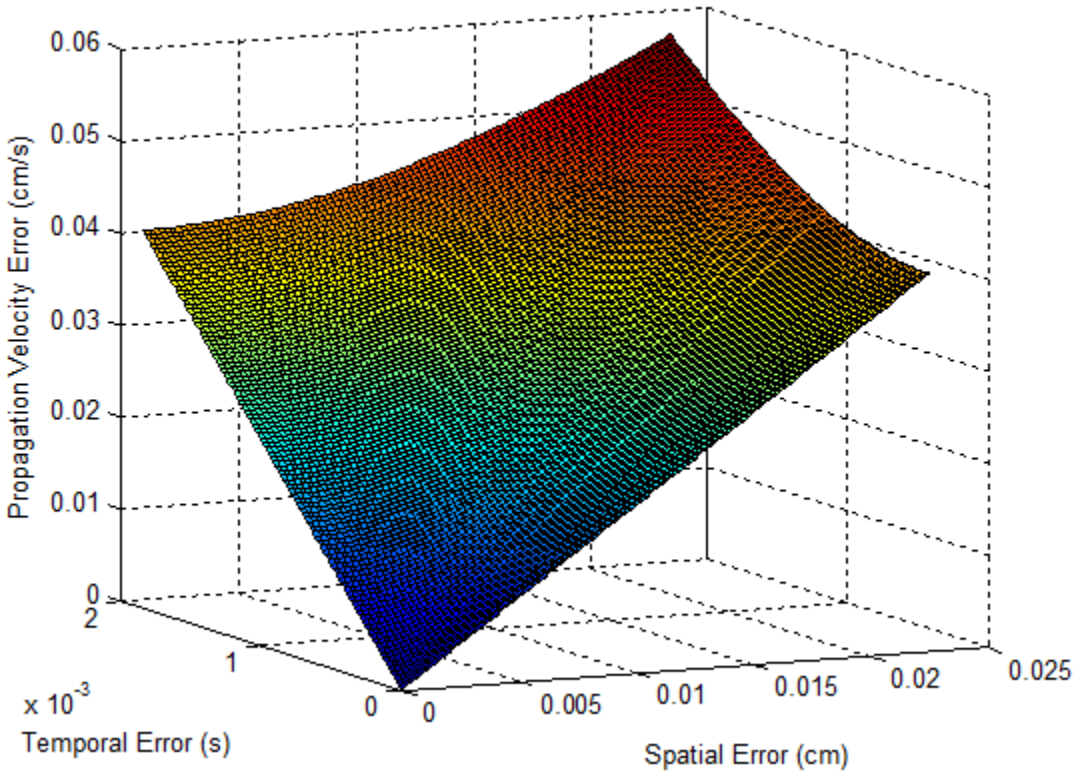

Figure 3.4: Slope error associated with varying both delta x and delta t

Basic Equation used in analysis:

$$\Delta p = -\rho\left(\frac{\Delta v}{\Delta t} + v\frac{\Delta v}{\Delta x}\right) + \mu\left(\frac{\Delta v}{\Delta x}\right)^2 \qquad 3.4$$

Associated Error:

$$\delta\Delta p = \left|\left(\frac{\partial\Delta p}{\partial\Delta x}\right)\delta\Delta x\right| + \left|\left(\frac{\partial\Delta p}{\partial\Delta t}\right)\delta\Delta t\right| + \left|\left(\frac{\partial\Delta p}{\partial\Delta v}\right)\delta\Delta v\right| \quad 3.5$$

$$\left(\frac{\partial\Delta p}{\partial\Delta x}\right) = -\frac{\mu 2\Delta v^2}{\Delta x^3} + \frac{\rho v\Delta v}{\Delta x^2} \quad 3.6$$

$$\left(\frac{\partial\Delta p}{\partial\Delta t}\right) = \frac{\rho\Delta v}{\Delta t^2} \quad 3.7$$

$$\left(\frac{\partial\Delta p}{\partial\Delta v}\right) = \frac{2\mu\Delta v}{\Delta x^2} - \rho\left(\frac{1}{\Delta t} + \frac{v}{\Delta x}\right) \quad 3.8$$

$$\delta\Delta p = \sqrt{\left(-\frac{\mu 2\Delta v^2}{\Delta x^3} + \frac{\rho v\Delta v}{\Delta x^2}\right)^2 (\delta\Delta x)^2 + \left(\frac{\rho\Delta v}{\Delta t^2}\right)^2 (\delta\Delta t)^2 + \left(\frac{2\mu\Delta v}{\Delta x^2} - \rho\left(\frac{1}{\Delta t} + \frac{v}{\Delta x}\right)\right)^2 (\delta\Delta v)^2} \quad 3.9$$

This relative pressure error $\delta\Delta p$ is calculated based on the error associated with the difference in pressures, difference in time, and difference in length and is evaluated using average pixel height and duration 0.045cm and 0.0034s. The range of δΔt and δΔx are 0 to half the mean temporal or spatial duration of the pixel respectively. The velocity value used in the calculation is a unit velocity of 1 m/s and the error associated with this velocity measurement is 0 to 33% of the total velocity. Figure 3.5,Figure 3.6, and Figure 3.7 display the errors in pressure measurement with the associated spatial, temporal, and velocity errors.

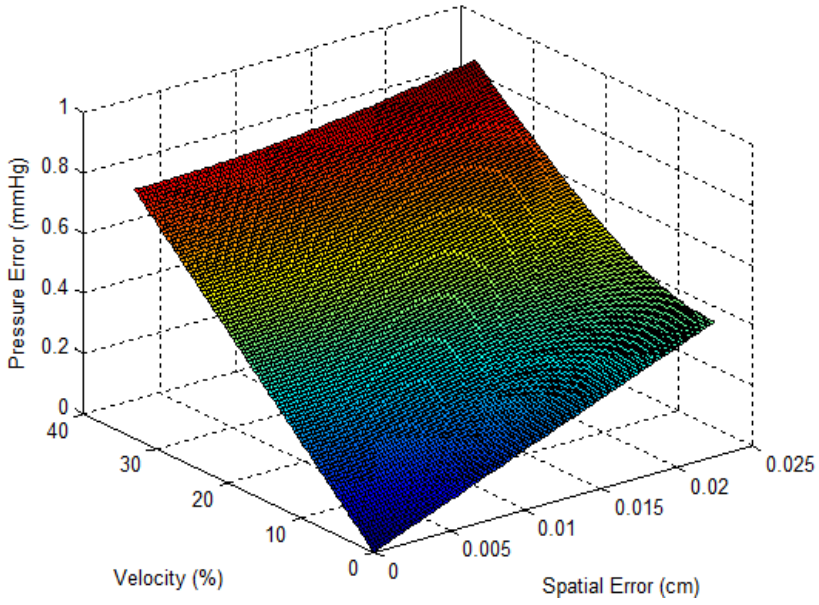

Figure 3.5: Pressure Error associated with velocity and spatial errors

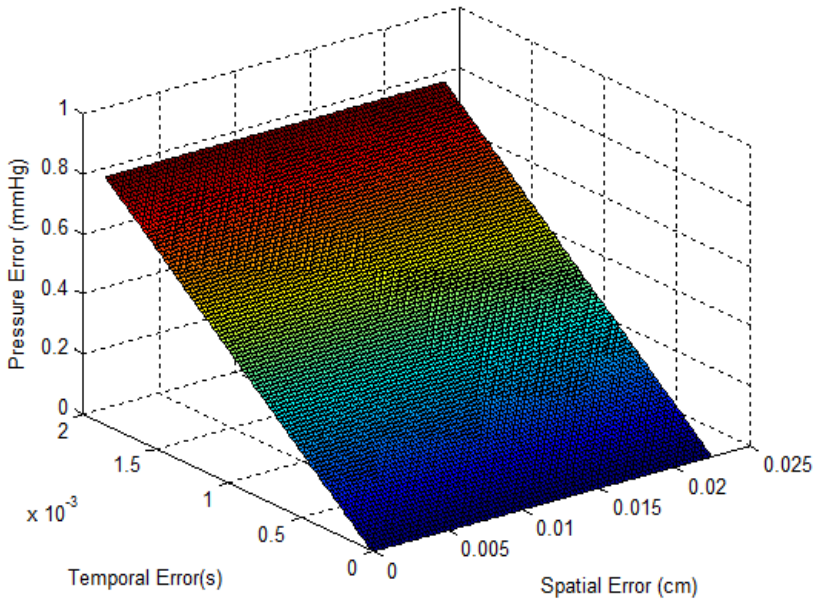

Figure 3.6: Pressure Error associated with temporal and spatial errors

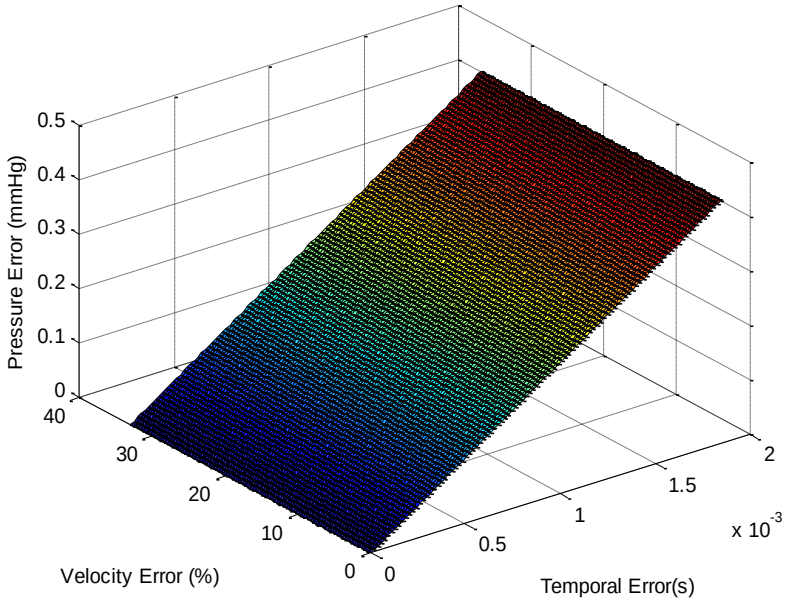

Figure 3.7: Pressure Error associated with velocity and temporal errors

Appendix B: Efficiency Work and L/D work

This section of the appendix displays preliminary work on other efficiency parameters not included in the body of the thesis as well as work based on formation number studies.

Background

Cardiac flows are by nature intricate involving unsteadiness, anisotropy, and transition to turbulence. In the presence of a diseased condition, the complexity of the flow is further increased and the pumping efficiency of the left heart is compromised. These flow physics are very difficult to understand using current clinical data acquisition.

There are four stages of diastolic dysfunction caused by both normal aging and diseased conditions. The first stage, stage 0, is healthy or normal LV filling. In a healthy heart, the early diastole, filling due to LV suction, encompasses about two thirds of the total filling causing the peak transmitral velocity ratio of E wave to A wave (E/A wave ratio) to be greater than one [1, 2]. The next stage, Stage 1, characterized by delayed relaxation. In this stage patients have a delayed rate of LV relaxation but their LV compliance and filling pressures are close to normal, therefore patients rarely see symptoms of diastolic dysfunction. Pseudonormal LV filling is labeled as Stage 2. Symptoms during this stage become more apparent such as enlargement of the heart. Although the signs at this stage closely follow those of normal left ventricular filling, they have subtle yet noticeable differences. The LV filling rate and compliance are slightly reduced and the filling pressures are slightly increased. The E/A wave ratio elevates to between one and two due to the great increase in E wave velocity because of the pressure increase. The final stage, Stage 3, of diastolic dysfunction is restrictive filling. The signs and symptoms of this stage are drastic. The LV filling pressure elevates and the compliance of the LV as well as the rate of left ventricular relaxation are severely reduced. Moderate to extreme LV enlargement is often seen in this stage and the E/A ratio is normally greater than two [3-7].

Currently, the most commonly used and useful technique for the diagnosis of heart failure is the echocardiogram [8, 9], which is the methodology used in this study. The diagnosis of diastolic dysfunction is often much more difficult than the diagnosis of systolic dysfunction using common echocardiography technology [8], which creates the drive for more physiologically accurate parameters to specifically understand the decline of diastolic function.

In recent years there has been increasing controversy over the methodology and procedure for calculating the early diastolic propagation velocity which is used in some efficiency parameters from color M-mode images. The propagation velocity measurement is a method of noninvasively quantifying the velocity of the incoming blood flow traveling from the mitral valve to the apex during early or late diastole. This velocity measurement captures the velocity of the propagating vortex ring and does not capture the velocity of the individual fluid particles within the vortex [10]. The alignment of the CMM scanline has been investigated to verify the propagation velocity calculated from the echocardiography is in fact the velocity of the propagating vortex ring. Greenberg et al. conducted a study to compare values obtained from echocardiograph images to velocity and pressure values generated by their numerical simulation. The results showed that a scanline positioned within the center 60% of the mitral valve will generate resultant values with a very small error compared to actual values [11-13].

The ejection fraction (EF) parameter has been previously considered as a functional parameter of left ventricular efficiency. The ejection fraction is the ratio of the volume of blood ejected from the LV during systole, or stroke volume, to the volume of blood in the LV at the end of diastole. This value can be easily obtained by assuming a symmetric ventricle and measuring the left ventricular end diastolic volume (LVEDV) and left ventricular end systolic volume (LVESV) from two dimensional echocardiograms [6]. Unfortunately, this parameter solely measures the percentage of ejection of the heart and is not directly linked to the severity of diastolic heart failure due to the heart's compensation

methods [6, 14]. Owan et al. conducted a research study at the Mayo Clinic Hospital in Minnesota to determine if there is a trend of heart failure patients' conditions over the past 15 years. The study found that the prevalence of heart failure has not changed over the time period but the percentage of heart failure patients with a healthy ejection fraction has drastically increased from thirty-eight percent to fifty-four percent from 1987 through 2001. It was the researchers' belief that this rise in the percentage of heart failure patients with preserved ejection fraction may have been due to the increasing number of patients with heart failure due to specific diseases such as, hypertension, atrial fibrillation and diabetes [15]. This change in the prevalence of heart failure with healthy ejection fraction may explain how the ejection fraction was once a parameter to diagnose ventricular efficiency but is currently not a reliable parameter for diagnosis.

Previously, parameters characterizing cardiac function have been developed with varying successes. Kass et al. calculated a maximal ventricular power term to track the LV systolic contractility. This term was the product of the instantaneous LV pressure and the change in LV volume with respect to time divided by the end diastolic volume squared. The power term was divided by the squared LV end diastolic volume to decrease the dependency on the preload [16]. Tei et al. described cardiac function by the combination of systolic and diastolic performance; the drive for this parameter was based on the belief that systolic and diastolic abnormalities are often linked. His combined parameter was the sum of the isovolumetric contraction time and the isovolumetric relaxation time divided by the ejection time of LV outflow. The parameter was shown to be a moderate indicator of cardiac function. Unfortunately this parameter was introduced as an inclusive measurement of systolic and diastolic function but was only tested on healthy patients and patients suffering from primarily systolic dysfunction. The authors state that results shown should not be assumed correct for predominantly diastolic dysfunction [17]. An efficiency parameter to distinguish normal from diabetic hearts was developed by modeling the LV filling as a damped single harmonic oscillator. Zhang et al. used the kinematic filling efficiency index to detect a small but noticeable difference in diabetic versus healthy patients when clinically used echocardiograph parameters displayed no difference. The equation was primarily based on the relaxation or the oscillator's damping constant and relatively independent of the stiffness or spring constant in the model. The kinematic filling efficiency index was tested on diabetic hearts but the authors believe it will be equally effective in discriminating healthy from unhealthy hearts in other disorders but this has not been tested [18].

Gharib et al. developed a nondimensional time scale for the formation of vortex rings. Equation 3.10 displays the formation time based on a piston cylinder arrangement.

$$\frac{L}{D} = \frac{\left(1/t \int_0^t u_p \, dt\right) t}{D} \qquad 3.10$$

where L is the stroke length of the piston, D is the diameter of the piston, t is the duration of fluid ejection from the orifice, and u_p is the piston velocity. Gharib et al. showed that a vortex ring ejected from an orifice by a piston will continue to increase until the formation time (L/D) becomes about 4. At this point the vortex ring is at its most energetically optimal point and all fluid expelled past this point forms a trailing jet. This concept of a formation time is applied to the filling of the LV during early diastole. The mean blood velocity during the E wave, duration of the E wave, and mitral annulus diameter were found using CMM Doppler and pulsed-wave Doppler images. The formation number was calculated for a total of 80 patients with seven of these patients having dilated cardiomyopathy and the remaining were blind test cases. The study concluded that the blind test cases calculated values converge to a range of 3.3 to 5.5, and the few patients with dilated cardiomyopathy fall below this range [19, 20].

Most similarly to the current work, Pierrakos and Vlachos developed a hydrodynamic filling efficiency. This parameter was the product of a mitral valve efficiency and a vortex ring efficiency term. The efficiency of the mitral valve was calculated using the previously established Froude efficiency equation. The vortex ring efficiency was then developed using the classic efficiency equation of useful work divided by total work. This equation is similar to the efficiency parameter used to understand the mechanics of squid propulsion with wasted energy being $1/2\rho Q(U_D-U_s)^2$, where U_D is the velocity of blood downstream of the mitral valve and U_s is the velocity of the almost motionless blood surrounding the incoming propagating vortex ring [21-23]. This hydrodynamic efficiency is shown in equation 3.11:

$$\eta_{VR} = \frac{2U_D U_{VR}}{2U_D U_{VR} + U_D^2 - 2U_D U_S + U_S^2} \quad 3.11$$

where U_D = downstream fluid velocity, U_S = surrounding fluid velocity, U_{VR} = vortex propagation speed [21].

From the previous research on echocardiography derived efficiency parameters, there are limiting factors on the parameters restricting their usefulness in effectively characterizing the decline in LV efficiency. There is no currently used and trusted method for calculating the efficiency of the LV. Many previous efficiency parameters have not been tested on clinical echocardiograph data or have been only tested on a very limited number of patients. Of the parameters that have been tested on patient data, some are specific to systolic dysfunction or have only been validated on systolic dysfunction patients, which is not the basis of the current investigation.

In this work, two novel efficiency parameters are introduced to characterize the decline in LV diastolic function. The novel parameters are tested on a population of 125 patients including both healthy and diseased patients. The population of diseased patients includes equal number of patients from the three recognized stages of diastolic dysfunction and includes patients with both preserved and decreased ejection fractions. An automated algorithm for the analysis of CMM images is introduced to reduce the introduction of subjective assessment of the user and allows for a more consistent analysis of CMM images.

Methods

A newly developed automated algorithm was used to analyze the CMM images of the patients included in this study. The patients included in this study as well as the detailed development of this algorithm is described in Chapter 1.

Results

The ejection fraction for each patient included in this study is shown in Figure 3.8. This figure demonstrates that healthy patients have a high ejection fraction with a mean value of 0.59 ± 0.052. The diseased patients have a substantial increase in the range of ejection fractions for each diastolic dysfunction stage with an average value of 0.56 ± 0.13 for delayed relaxation, 0.39 ± 0.14 for pseudonormal, and 0.28 ± 0.074 for restrictive. There are many delayed relaxation and pseudonomal patients exhibiting a preserved ejection fraction.

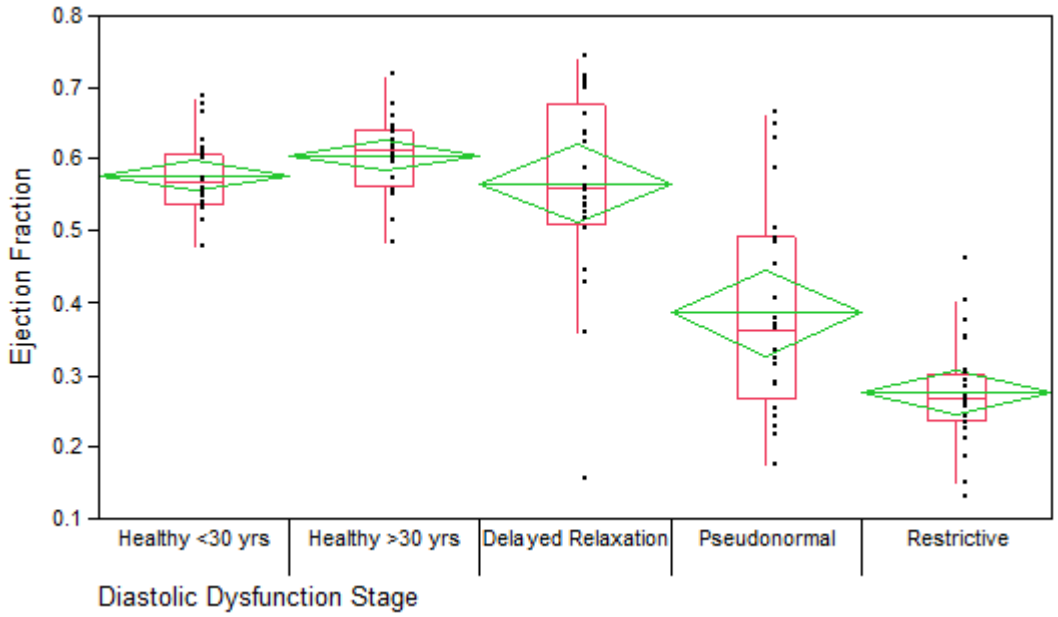

Figure 3.8: Ejection Fraction Values Shown by Diastolic Dysfunction Stage

The efficiency ratio of the early diastolic filling wave was calculated using a simple ratio of velocities. The filling efficiency is the comparison of the break point propagation velocity and the E wave transmitral velocity. Although this ratio is simplistic, it incorporates multiple aspects of the filling including the pressure distribution within the left ventricle and the compliance of the left ventricle. The rate of kinetic energy entering the system is $1/2\rho QV_E^2$ where V_E is the transmitral velocity and the rate of useful energy is $1/2\rho QV_P^2$ where V_P is the propagation velocity. The ratio of velocities is arranged in this way due to the basic efficiency equation of useful work divided by total work. In this situation the useful work is defined as the rate of energy in the propagating vortex ring and the total work is the energy at the mitral valve during diastole.

The reciprocal of this ratio has been investigated previously and correlates well with LV end diastolic pressure. Patients with a transmitral E wave velocity to propagation velocity ratio greater than 1.5 are said to have increased filling pressures [24]. The current analysis views the reciprocal of this previously introduced as a new hydrodynamic parameter to characterize the efficiency of early diastolic filling.

The analysis of an ideal slug flow through an orifice which produces a propagating vortex ring is very similar to this efficiency parameter. In ideal conditions, assuming a thin ring vortex approximation it can be shown that the velocity of the propagating vortex ring is ½ the velocity of the fluid at the orifice [25]. It is assumed that a patient with healthy left ventricular filling will most closely resemble these ideal conditions. The intraventricular pressure difference and compliance of the LV allow the jet to travel from the orifice of the mitral valve towards the left ventricular apex with little resistance in order to most efficiency fill the ventricle. Figure 3.9 shows healthy patients exhibit a mean diastolic efficiency ratio of 60.0 ± 12.3%, following the trend of ideal downstream jet velocity very closely. As the diastolic function of the patients decreases, there is a decrease in the ratio of propagation velocity to E wave transmitral velocity. The combination of the decrease in passive relaxation of the ventricle, the increase in stiffness of the LV, and the decrease in intraventricular pressure difference causes the filling efficiency to decrease. The restrictive filling case has a mean diastolic efficiency ratio of only 31.2 ± 10.7%, displaying a substantial decrease in propagation velocity with respect to transmitral velocity as

compared to the healthy filling patients. The wasted energy is the energy transferred into the fluid that is not used towards moving the fluid towards the apex. This energy is transferred to rotation energy and viscous dissipation and off axis velocity.

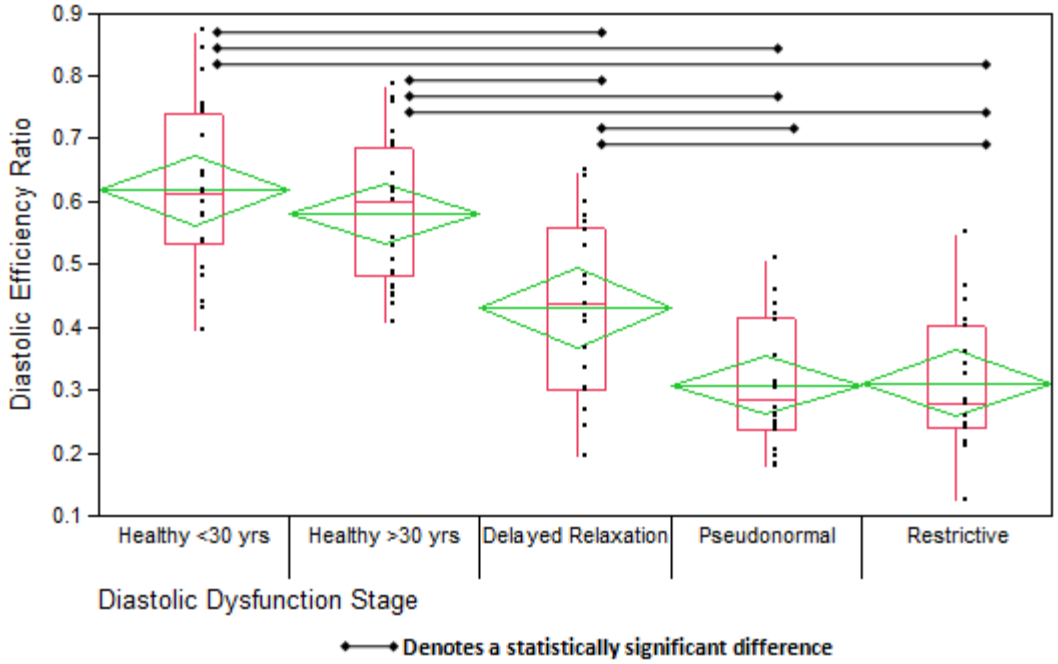

Figure 3.9: Diastolic Efficiency Radius and Ventricular Power Parameter

A second measurement of diastolic efficiency is the ventricular diastolic power. This parameter is the product of the peak mitral to apical pressure difference, the break point propagation velocity, and the square of the characteristic length of the ventricle. The characteristic length is defined in equation 3.12:

$$L_c = \sqrt[3]{LVEDV} - \sqrt[3]{LVESV} \tag{3.12}$$

The characteristic length is the change in the length scale during the relaxation of the LV from the end of diastole to the end of systole assuming the LV is a cube. This characteristic length is squared to represent the LV change in area. The LV diastolic power equation is shown in equation 3.13, where the ΔP_{LV} is the peak mitral to apical pressure difference during the E wave, V_p is the critical propagation velocity calculated in chapter 1, and L_c is the newly introduced characteristic length.

$$P_D = \Delta P_{LV} V_p {L_c}^2 \tag{3.13}$$

The ventricular power parameter declines as the peak mitral to apical pressure difference, the propagation velocity and characteristic length based on the geometrical change during diastole decreases. This parameter incorporates the three important parameters to the filling of early diastole, pressure difference, inflow velocity, and ventricular relaxation. The ventricular power parameter is plotted against the diastolic dysfunction stage in Figure 3.10.

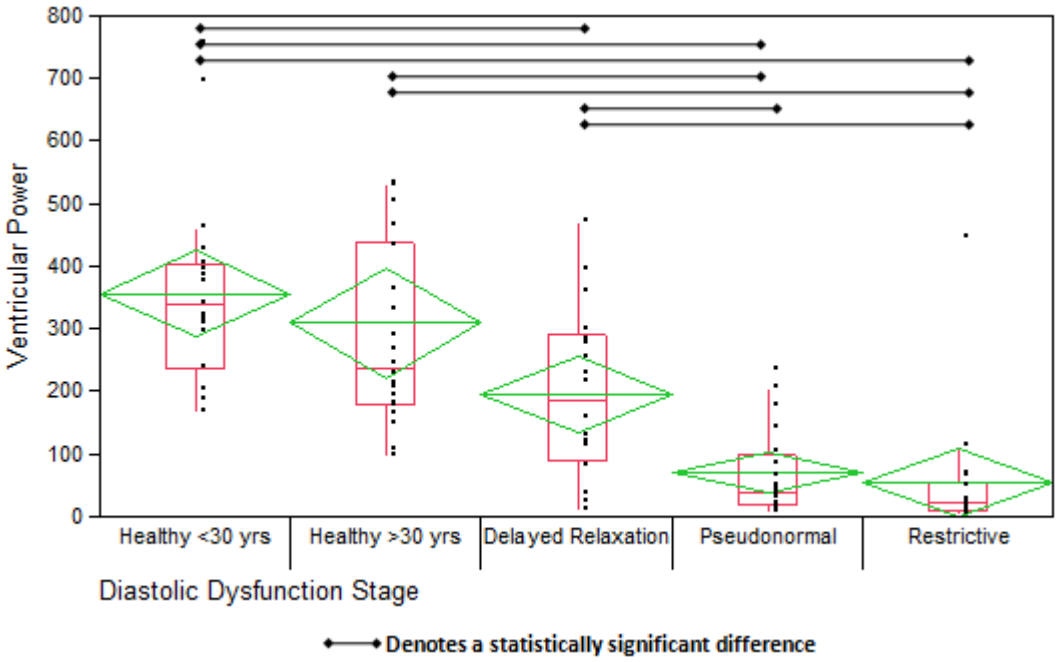

Figure 3.10: Left Ventricular Diastolic Power shown by Diastolic Dysfunction Stage

A severe reduction in all three of the parameters is present in restrictive filling patients with an average ventricular power of 54.8 ± 105.0. In these cases there is a very weak suction within the ventricle, a very slow inflow velocity and little ventricular relaxation during diastole. The decline of the ventricular power value is an indication of the decline of useful work used for the filling of the early diastolic wave. As this value decreases, there is an increase in energy lost to other means not directly related to diastolic filling, such as viscous dissipation, off axis velocity, and rotational energy.

The formation number, equation 3.10, is estimated using the mean E wave velocity estimated from CMM images, the duration of the E wave estimated from pulse wave Doppler images, and the mitral valve diameter at diastasis measured using a 4-chamber Echocardiograph image. The formation number for each patient in this study is shown in Figure 3.11A. The healthy patients have a mean L/D of 4.3 ± 0.17, which is analogous to the most efficient range of formation numbers as presented by Gharib et al. [20]. Restrictive filling patients show a L/D value of 2.9 ± 0.18 demonstrating a less efficiency vortex ring propagating toward the apex. Figure 3.11B presents the L/D values plotted by age, there is an inverse correlation of L/D with respect to age regardless of diastolic dysfunction stage. The solid black line represents the trend line of this correlation with the dashed black lines and shaded region showing a single standard deviation of this trend. A group of restrictive filling patients ages 40 to 70 years old is plotted below the one standard deviation prediction interval, this indicates that the inverse correlations found in Figure 3.11 A and B is not independently based on age or diastolic dysfunction stage but a combination of both. Gharib et al. introduced this parameter as a method for the diagnosis of DCM patients showing healthy patients with values between 3.5 and 5.5 varying with age and DCM patients below 3. This diagnostic parameter does not hold true for patients with varying stages of diastolic dysfunction, because healthy patients as well as patients with delayed relaxation and pseudonormal filling follow the subtle trend of decreasing L/D with age within the bounds of healthy patients as introduced by Gharib et al. [20].

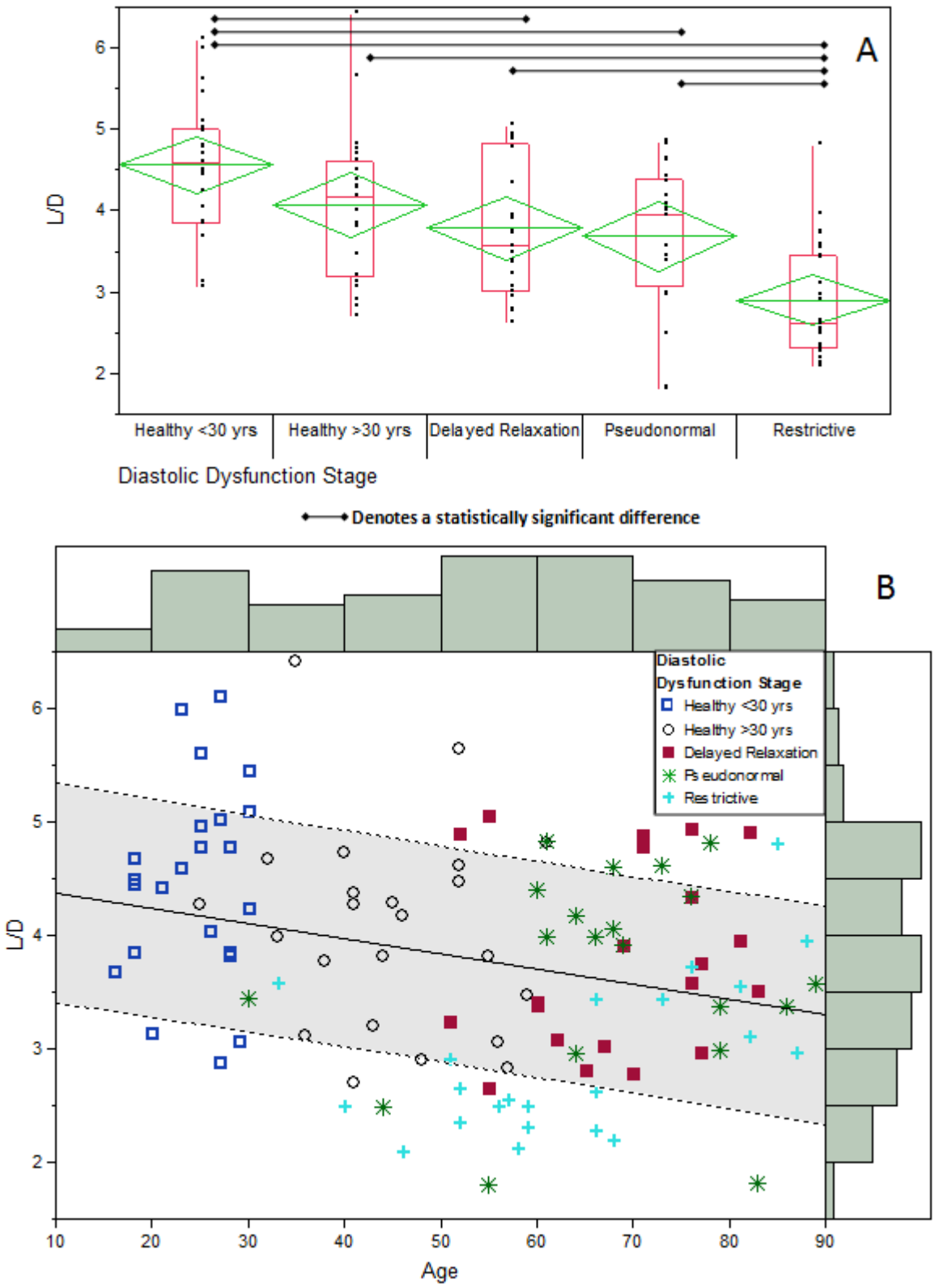

Figure 3.11: Formation Number plotted by Diastolic Dysfunction Stage and Age

Discussion

This study introduces two novel efficiency parameters for the analysis of the decline of diastolic dysfunction. The parameters examine the amount of work utilized in the filling of the LV during early diastole. These two efficiency parameters are compared to one of the most commonly used ratios for the diagnosis of diastolic dysfunction, E/E'. Figure 3.12 displays the dynamic efficiency parameter and ventricular power parameter plotted against the E/E' parameter, displaying a one standard deviation prediction contour per diastolic dysfunction stage. It is noteworthy that the classification of these patients was moderately based on the value of E/E' but the pseudonormal and restrictive cases display a lower standard deviation for the two new parameters then for the E/E' parameter. The E/E' parameter exhibits a much smaller standard deviation in the healthy classes then the new parameters; however, the new parameters, especially the dynamic efficiency ratio show a much smaller standard deviation then the E/E' parameter on the diseased patients. For both efficiency parameters there is a trend of decreasing efficiency with increasing E/E'. There are very few patients with high E/E' and high efficiency, indicating as the ratio of E peak transmitral velocity to E peak mitral annulus velocity increases due to decreased relaxation and stiffening of the LV, the efficiency is also decreasing. The introduction of one or both of these efficiency parameters into the clinically used diagnostic parameter has the capability to have a large impact on the understanding of diastolic dysfunction.

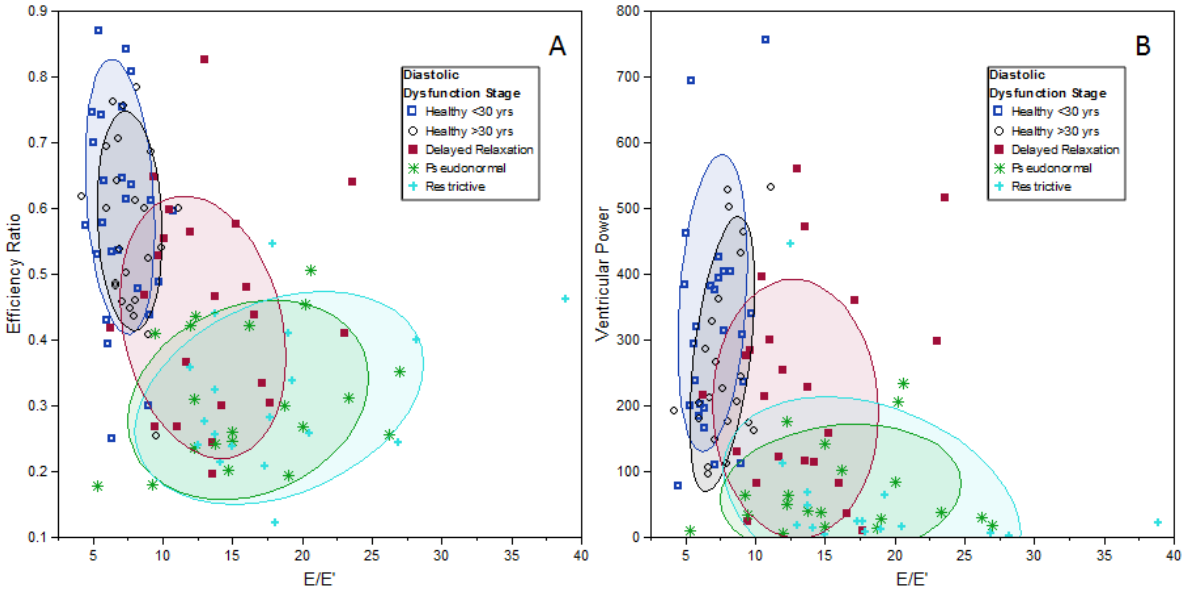

Figure 3.12: Dynamic Efficiency Ratio and Ventricular Power vs. E/E'

The efficiency ratio parameter displays a clear separation between healthy and severely diseased patients. There are a few delayed relaxation patients within the prediction region for healthy patients; unfortunately without long term survival studies of these patients there is no assurance that these patients do undeniably have delayed relaxation filling. The one standard deviation prediction region for both efficiency parameters show some degree of separation between healthy and severely diseased and exhibit overlap between young and older healthy patients and pseudonormal and restrictive filling patients. This demonstrates that although some parameters change in healthy patients as age increases the useful work incorporate employed in early diastolic filling is generally the same and the efficiency of the E wave is still high regardless of age. Also, the efficiency of the E wave during pseudonormal filling and restrictive filling is nearly identical for the majority of patients studied. While the heart is compensating and remodeling to create the pseudonormal filling stage as similar as obtainable to

healthy filling the efficiency of the E wave filling of this stage is equivalent to restrictive filling efficiency. The pseudonormal filling is mimicking healthy filling but is utilize severely less constructive energy and therefore a larger percentage of energy is transferred to fluid movements not aiding E wave filling.

Conclusions

Clinical CMM images were utilized for the introduction of two novel efficiency parameters. The diastolic efficiency ratio was displayed as a ratio of useful work to total work imputed into the left ventricle during the early filling wave of diastole. The reciprocal of this ratio has been previously introduced but has never before been viewed as an efficiency of early diastole. The second efficiency parameter was the left ventricular diastolic power term. This parameter calculates the power as a product of the peak mitral to apical pressure difference, the break point propagation velocity and the squared characteristic length. The two newly introduced efficiency parameters display a decrease in useful work moving the blood from the mitral valve towards the apex as the diastolic function of the patients' decreases. The parameters indicate that the E wave efficiency of healthy patients is unaltered by age and the efficiency of pseudonormal and restrictive filling are nearly equivalent. The formation number was calculated for the patients studied and shown to correlate with both diastolic dysfunction stage and age. The two efficiency parameters are based on the physical understanding of the decline of efficiency of an unhealthy heart, which gives these parameters promise for being clinically useful in the understanding of the decline of diastolic dysfunction.

References

1. Takatsuji, H., et al., A new approach for evaluation of left ventricular diastolic function: Spatial and temporal analysis of left ventricular filling flow propagation by color M-mode Doppler echocardiography. Journal of the American College of Cardiology, 1996. 27(2): p. 365-371.
2. Greenberg, N.L., et al., *Estimation of diastolic intraventricular pressure gradients by Doppler M-mode echocardiography.* American Journal of Physiology-Heart and Circulatory Physiology, 2001. 280(6): p. H2507-H2515.
3. Palecek, T., et al., Early diastolic mitral annular velocity and color M-mode flow propagation velocity in the evaluation of left ventricular diastolic function in patients with Fabry disease. Heart and Vessels, 2006. 21(1): p. 13-19.
4. De Mey, S., et al., Assessment of LV Diastolic Filling Using Color M-Mode Doppler Echocardiography: Validation in a New Hydraulic Model, in Biomechan Model Mechanobiol. 2004. p. 127-138.
5. Ommen, S.R., et al., Clinical utility of Doppler echocardiography and tissue Doppler imaging in the estimation of left ventricular filling pressures - A comparative simultaneous Doppler-Catheterization study. Circulation, 2000. 102(15): p. 1788-1794.
6. Thomas, J.D. and Z.B. Popovic, *Assessment of left ventricular function by cardiac ultrasound.* Journal of the American College of Cardiology, 2006. 48(10): p. 2012-2025.
7. Garcia, M.J., J.D. Thomas, and A.L. Klein, *New Doppler echocardiographic applications for the study of diastolic function.* Journal of the American College of Cardiology, 1998. 32(4): p. 865-875.
8. Oh, J.K., *Echocardiography in heart failure: Beyond diagnosis.* European Journal of Echocardiography, 2007. 8(1): p. 4-14.
9. Parthenakis, F.I., et al., Late left ventricular diastolic flow propagation velocity determined by color M-mode Doppler in the assessment of diastolic dysfunction. Journal of the American Society of Echocardiography, 2004. 17(2): p. 139-145.
10. Claessens, T.E., et al., New echocardiographic applications for assessing global left ventricular diastolic function. Ultrasound in Medicine and Biology, 2007. 33(6): p. 823-841.
11. Greenberg, N.L., et al. Significance of color Doppler M-mode scanline orientation in the non-invasive assessment of intraventricular pressure gradients. in 24th Annual Computers in Cardiology Conference. 1997. Lund, Sweden.
12. Greenberg, N.L., et al. Effect of scanline orientation on ventricular flow propagation: Assessment using high frame-rate color Doppler Echocardiography. in 37th Annual Rocky Mountain Bioengineering Symposium/37th International ISA Biomedical Sciences Instrumentation Symposium. 2000. Colorado Springs, Co.
13. De Boeck, B.W.L., et al., Colour M-mode velocity propagation: a glance at intra-ventricular pressure gradients and early diastolic ventricular performance. European Journal of Heart Failure, 2005. 7(1): p. 19-28.
14. Brucks, S., et al., Contribution of left ventricular diastolic dysfunction to heart failure regardless of election fraction. American Journal of Cardiology, 2005. 95(5): p. 603-606.
15. Owan, T.E., et al., *Trends in prevalence and outcome of heart failure with preserved ejection fraction.* New England Journal of Medicine, 2006. 355(3): p. 251-259.
16. Kass, D.A. and R. Beyar, EVALUATION OF CONTRACTILE STATE BY MAXIMAL VENTRICULAR POWER DIVIDED BY THE SQUARE OF END-DIASTOLIC VOLUME. Circulation, 1991. 84(4): p. 1698-1708.

17. Tei, C., et al., New Index of Combined Systolic and Diastolic Myocardial Performance: A Simple and Reproducible Measure of Cardiac Function - A Study in Normals and Dilated Cardiomyopathy. Journal of Cardiology, 1995. 26: p. 357-366.
18. Zhang, W., et al., The kinematic filling efficiency index of the left ventricle: Contrasting normal vs. diabetic physiology. Ultrasound in Medicine and Biology, 2007. 33(6): p. 842-850.
19. Gharib, M., E. Rambod, and K. Shariff, *A universal time scale for vortex ring formation.* Journal of Fluid Mechanics, 1998. 360: p. 121-140.
20. Gharib, M., et al., *Optimal vortex formation as an index of cardiac health.* Proceedings of the National Academy of Sciences of the United States of America, 2006. 103(16): p. 6305-6308.
21. Pierrakos, O. and P.P. Vlachos, *The effect of vortex formation on left ventricular filling and mitral valve efficiency.* Journal of Biomechanical Engineering-Transactions of the Asme, 2006. 128(4): p. 527-539.
22. Prandtl, L., *Essentials in Fluid Dynamics*. 1952, London: Blackie & Son,.
23. Anderson, E.J. and M.E. Demont, The mechanics of locomotion in the squid Loligo pealei: Locomotory function and unsteady hydrodynamics of the jet and intramantle pressure. Journal of Experimental Biology, 2000. 203(18): p. 2851-2863.
24. Moller, J.E., et al., Ratio of left ventricular peak E-wave velocity to flow propagation velocity assessed by color M-mode Doppler echocardiography in first myocardial infarction - Prognostic and clinical implications. Journal of the American College of Cardiology, 2000. 35(2): p. 363-370.
25. Shusser, M., M. Gharib, and K. Mohseni, A New Model For the Inviscid Vortex Ring Formation in American INstitude of Aeronautics & Astronautics. 30th AIAA Fluid Dynamics Conference. 1999: Norfolk, VA.